Atmos. Chem. Phys. Discuss., 14, 22385–22435, 2014
www.atmos-chem-phys-discuss.net/14/22385/2014/
doi:10.5194/acpd-14-22385-2014
© Author(s) 2014. CC Attribution 3.0 License.

Atmospheric Chemistry and Physics Discussions
Open Access

This discussion paper is/has been under review for the journal Atmospheric Chemistry and Physics (ACP). Please refer to the corresponding final paper in ACP if available.

# Influence of isoprene chemical mechanism on modelled changes in tropospheric ozone due to climate and land use over the 21st century

**O. J. Squire[1], A. T. Archibald[1,2], P. T. Griffiths[1,2], M. E. Jenkin[3], and J. A. Pyle[1,2]**

[1]Centre for Atmospheric Science, Department of Chemistry, University of Cambridge, Cambridge, CB2 1EW, UK
[2]National Centre for Atmospheric Science, Department of Chemistry, University of Cambridge, Cambridge, CB2 1EW, UK
[3]Atmospheric Chemistry Services, Okehampton, Devon EX20 1FB, UK

Received: 7 July 2014 – Accepted: 5 August 2014 – Published: 1 September 2014

Correspondence to: O. J. Squire (ojsquire@gmail.com)

Published by Copernicus Publications on behalf of the European Geosciences Union.

## Abstract

Isoprene is a precursor to tropospheric ozone, a key pollutant and greenhouse gas. Anthropogenic activity over the coming century is likely to cause large changes in atmospheric $CO_2$ levels, climate and land use, all of which will alter the global vegetation distribution leading to changes in isoprene emissions. Previous studies have used global chemistry–climate models to assess how possible changes in climate and land use could affect isoprene emissions and hence tropospheric ozone. The chemistry of isoprene oxidation, which can alter the concentration of ozone, is highly complex, therefore it must be parameterised in these models. In this work we compare the effect of four different reduced isoprene chemical mechanisms, all currently used in Earth-system models, on tropospheric ozone. Using a box model we compare ozone in these reduced schemes to that in a more explicit scheme (the MCM) over a range of $NO_x$ and isoprene emissions, through the use of $O_3$ isopleths. We find that there is some variability, especially at high isoprene emissions, caused by differences in isoprene-derived $NO_x$ reservoir species. A global model is then used to examine how the different reduced schemes respond to potential future changes in climate, isoprene emissions, anthropogenic emissions and land use change. We find that, particularly in isoprene rich regions, the response of the schemes varies considerably. The wide ranging response is due to differences in the types of peroxy radicals produced by isoprene oxidation, and their relative rates of reaction towards NO, leading to ozone formation, or $HO_2$, leading to termination. Also important is the yield of isoprene-nitrates and peroxyacyl nitrate precursors from isoprene oxidation. Those schemes that produce less of these $NO_x$ reservoir species, tend to produce more ozone locally and less away from the source region. Additionally, by combining the emissions and $O_3$ data from all of the global model integrations, we are able to construct isopleth plots comparable to those from the box model analysis. We find that the global and box model isopleths show good qualitative agreement, suggesting that comparing chemical mechanisms with a box model in this framework is a useful tool for assessing mechanistic






ACPD
14, 22385–22435, 2014

performance in complex global models. We conclude that as the choice of reduced isoprene mechanism may alter both the magnitude and sign of the ozone response, how isoprene chemistry is parameterised in perturbation experiments such as these is a crucially important consideration. More measurements are needed to validate these reduced mechanisms especially in high-VOC, low-$NO_x$ environments.

## 1 Introduction

The emission of volatile organic compounds (VOCs) into the atmosphere under the presence of $NO_x$ (the sum of nitric oxide (NO) and nitrogen dioxide ($NO_2$)) can lead to the formation of tropospheric ozone ($O_3$), which is a pollutant and greenhouse gas (e.g. Haagen-Smit, 1952). One VOC that contributes significantly to tropospheric $O_3$ production is the biogenically emitted di-alkene isoprene (2-methyl-1,3-butadiene) with annual emissions of $\sim 500\,\mathrm{Tg\,C}$ (Guenther et al., 2006). Isoprene is highly reactive with an atmospheric lifetime on the order of about 1–2 h, and thus has the potential to strongly influence levels of tropospheric $O_3$ both regionally (e.g. Chameides et al., 1988) and globally (e.g. Wang and Shallcross, 2000).

Isoprene is oxidised in the atmosphere by the hydroxyl radical (OH), $O_3$ and the nitrate radical ($NO_3$). These reactions initiate a complex cascade of photochemical interactions, which (theoretically) comprise of $> 10^5$ reactions involving $> 10^4$ species (Aumont et al., 2005). Including all of these reactions in 3-D global modelling studies is too computationally expensive and so isoprene chemistry must be parameterised. Furthermore, our understanding of isoprene oxidation is incomplete; only a small number of these $10^5$ reactions are known fundamentally. Although parameterisation is a necessity, it introduces uncertainties in the chemistry and subsequent calculation of trace gas composition, as multiple species or reactions have to be lumped together. Furthermore, there are several different methodologies for how best to parameterise an explicit chemical mechanism, which has led to the existence of a plethora of different reduced schemes, whose use in models can lead to different results (e.g. Archibald





ACPD
14, 22385–22435, 2014

et al., 2010b). Jeffries et al. (1992) laid out a set of basic considerations to make when evaluating a condensed chemical mechanism, which are the points in the process of condensed mechanism development where individual methodologies may diverge. These include the relationship between different lumping groups and explicit species, the method used to select individual lumping groups, e.g. by characteristic reaction times, molecular weight or chemical structure, and the approach to handling chain degradation kinetics for each lumped species. The choices made in developing reduced mechanisms may also have been made with the aim of accurately representing specific timescales (e.g. urban or continental) or species (e.g. $O_3$) (Jeffries et al., 1992).

To date there have been several studies that calculate the effects of future isoprene emission changes caused by potential climate and land use scenarios on surface $O_3$ (Sanderson et al., 2003; Wiedinmyer et al., 2006; Ganzeveld et al., 2010; Wu et al., 2012; Pacifico et al., 2012), including our recent study (Squire et al., 2014). These 3-D global modelling studies all use (often different) reduced isoprene mechanisms, however very few studies have attempted to quantify the influence of variation in the isoprene scheme on the $O_3$ response. Previously, von Kuhlmann et al. (2004) did compare two different isoprene mechanisms and related parameters such as the deposition of intermediates, the treatment of isoprene-nitrates and the emission strength of $O_3$ precursors, all within a particular global model. Here we explore the behaviour of four reduced schemes, all designed to run in complex Earth System Models (ESMs), in the context of the climate and land use perturbation experiments carried out in Squire et al. (2014). Given the importance of $O_3$ in the Earth system (Huntingford et al., 2011) our analysis focuses specifically on $O_3$ and on $O_3$ precursors.

Even without mechanism reduction there exist sources of uncertainty in isoprene oxidation, which are associated with our fundamental lack of understanding about certain aspects of the chemistry. One such aspect is the degree to which $HO_x$ is regenerated from isoprene degradation under low $NO_x$-high VOC conditions. Several campaigns in such conditions (GABRIEL, Kubistin et al., 2010; INTEX-A, Ren et al.,





ACPD
14, 22385–22435, 2014

2008; OP3, Stone et al., 2011; Whalley et al., 2011) reported levels of $HO_x$ that were higher than expected, considering the high reactivity of isoprene with OH ($k_{298K}$ = $10^{-10}$ $cm^3$ $molecule^{-1}$ $s^{-1}$). Proposals have been put forward for missing mechanistic pathways, e.g. peroxy radical isomerisation (Peeters et al., 2009), and epoxide formation (Paulot et al., 2009) which to some extent reconcile these discrepancies (Archibald et al., 2010a; Warwick et al., 2013; Fuchs et al., 2013). It has also been demonstrated that positive biases in the measurement of $HO_2$ (Fuchs et al., 2011) and OH (Mao et al., 2012) cannot be ruled out in some of those field campaigns listed above. Mao et al. (2012) found that, for a Californian forest environment, taking into account these biases in addition to the proposed mechanistic pathways, gave good agreement between modelled and measured $HO_x$.

Another source of uncertainty is in the chemistry of isoprene nitrates. When hydroxyperoxy radicals from OH-initiated isoprene oxidation ($ISO_2$) react with NO, the major pathway leads to the formation of alkoxy radicals and $NO_2$ (leading to $O_3$ formation). However, there is a minor channel that leads to the formation of isoprene nitrates, which act to sequester $NO_x$. There are several uncertainties surrounding the chemistry of isoprene nitrates. Firstly, estimates of the yield of isoprene nitrates from the OH/NO channel range from 4.4 to 15 % (Xie et al., 2013, and references therein). Modelling studies have shown that the assumed yield of isoprene nitrates can have a large impact on tropospheric $O_3$ (e.g. von Kuhlmann et al., 2004; Wu et al., 2007; Paulot et al., 2012). Secondly, isoprene nitrates may also be formed from the oxidation of isoprene by $NO_3$, which is estimated to account for 30–60 % of isoprene nitrate production (von Kuhlmann et al., 2004; Horowitz et al., 2007; Paulot et al., 2012). The types of isoprene nitrates formed via the $NO_3$ pathway are distinct from those formed via the OH/NO pathway and details of their atmospheric fates remain relatively obscure (Xie et al., 2013). Thirdly, once formed, isoprene nitrates are readily photooxidised (lifetime ~ 4 h with respect to OH (OH = $10^6$ molecule $cm^{-3}$)), leading either to release of $NO_x$, or to second generation nitrates, retaining the nitrate group. The degree to which $NO_x$ is regenerated from isoprene nitrate degradation remains uncertain (Fiore et al., 2012;





ACPD
14, 22385–22435, 2014



CC BY

Xie et al., 2013) and has a significant effect on the $O_3$ response to isoprene emission changes (Paulot et al., 2012). Fourthly, dry deposition of isoprene nitrates, which could represent an important $NO_x$ sink in isoprene-rich regions, is also uncertain, with measured deposition velocities ranging from 0.4 cm $s^{-1}$ (Shepson et al., 1996) to 2.7 cm $s^{-1}$ (Farmer and Cohen, 2008). Finally, there has been recent evidence for the importance of $O_3$-initiated isoprene nitrate degradation (Lockwood et al., 2010; Lee et al., 2014) and fast photolysis of isoprene nitrates (Müller et al., 2014). In this current study the isoprene schemes we compare have a range of different parameterisations for isoprene nitrates.

In Sect. 2 we describe in detail the chemical mechanisms used in this study and the methodology for the global perturbation experiments. In Sect. 3 we discuss the results of a series of box model simulations, with the aim of comparing our four reduced mechanisms to the Master Chemical Mechanism (MCM). This is done for a range of $NO_x$ and isoprene concentrations. Global integrations with each mechanism are then conducted to examine the effect of changes in climate, in isoprene emissions with climate, in anthropogenic emissions and in land use. In Sects. 4–6 we analyse the results of these global perturbation experiments.

## 2 Methods

In this section we outline the experiments conducted to ascertain the effect of using different reduced isoprene chemical mechanisms in the context of global climate, emissions and land use change experiments (Sect. 2.2.2). In Sect. 2.1 details of the reactions and species that make up the reduced mechanisms are given.

### 2.1 Isoprene chemical mechanisms

The species included in each mechanism are given in Table 1, whilst a comparison of the reactions is given in Table 2. The different isoprene mechanisms were each embed-





ACPD
14, 22385–22435, 2014



CC BY

ded in an otherwise identical tropospheric chemistry mechanism simulating the chemistry of methane, ethane, propane, $HO_x$ and $NO_x$, following O'Connor et al. (2014).

The first mechanism used was the UM-UKCA Chemistry of the Troposphere (CheT) mechanism, as used for all integrations in Squire et al. (2014). The CheT isoprene mechanism consists of 16 species and 44 reactions (see Tables 1 and 2), and is based on the Mainz Isoprene Mechanism (MIM) (Poschl et al., 2000). MIM was developed from a systematic reduction of the Master Chemical Mechanism (version 2) (Jenkin et al., 1997), by lumping species based on their structure (e.g. all hydroxyperoxy radicals were lumped as $ISO_2$, and methacrolein and methyl vinyl ketone as methacrolein, MACR). The overall CheT mechanism also forms the basis of all the schemes studied, with only the parts pertaining to isoprene being different.

Since the creation of MIM, there have been a number of developments in our understanding of isoprene chemistry, concerning issues such as those discussed in the introduction. In a report compiled for the UK Met Office (Jenkin, 2012), these new developments were also incorporated into the current CheT framework. The resulting updated mechanism (which will be referred to as CheT2, see Tables 1 and 2) is the most complex mechanism used in this current study, consisting of 24 species and 59 reactions, and is traceable to the MCM version 3.2 (MCMv3.2).

The following is a summary of the changes made from CheT to CheT2. Firstly, changes to the chemistry of first generation isoprene nitrates (ISON) were made. In CheT, $NO_x$ is regenerated from ISON by photolysis or conversion to second generation nitrates (NALD) followed by reaction with OH. In CheT2 the overall yield of $NO_x$ from ISON was increased, in line with recent measurements (Perring et al., 2009), by increasing the ISON photolysis rate and adding an $ISON + OH \rightarrow NO_2$ reaction channel. $O_3$ initiated degradation of ISON was also added based on the evidence of Lockwood et al. (2010). Secondly, CheT2 includes the formation of hydroperoxy-aldehydes (HPALDs) from $ISO_2$ and subsequent rapid release of OH (Peeters et al., 2009). This leads to more $HO_x$ regeneration in low $NO_x$ high isoprene conditions, bringing modelled and measured values closer together (e.g. Archibald et al., 2010a). The formation of





ACPD
14, 22385–22435, 2014

isoprene epoxydiols (IEPOX) from the oxidation of isoprene hydroxy-hydroperoxides (ISOOH), a potential source of secondary organic aerosols (Paulot et al., 2009), was also included in CheT2. Finally, the yield of peroxymethacrylic nitric anhydride (MPAN) from isoprene oxidation was revised down from its CheT value (Jenkin, 2012).

The Air Quality in the Unified Model (AQUM) scheme, which was developed to deliver regional air quality forecasts and conduct air quality studies to inform emission control policies (Savage et al., 2013) was also investigated. The mechanism has a more anthropogenic VOC focus and a less detailed isoprene scheme compared with CheT (17 species, 23 reactions). Two important simplifications in the isoprene scheme are that (1) isoprene nitrates are not formed from the OH initiated pathway via the reaction of $ISO_2$ with NO, and (2) there is no production of MPAN.

The last and most simple isoprene scheme used was the super-fast chemistry scheme developed at the Lawrence Livermore National Laboratory (LLSF) (Cameron-Smith et al., 2009) for use in the Community Earth System Model (CESM – http://www.cesm.ucar.edu/models/cesm1.0/). The LLSF isoprene scheme only considers the reactions of isoprene with OH and $O_3$, and was parameterised based on the net effect of a more complex isoprene mechanism (Cameron-Smith et al., 2009). Aside from not including isoprene chemistry at all, it is about as simple an approximation of isoprene chemistry as is currently used in ESMs, but is still a significant improvement over neglecting isoprene chemistry altogether (Cameron-Smith et al., 2009). The scheme was developed for use in very long global 3-D integrations, where reducing computational cost is paramount.

## 2.2 Model experiments

### 2.2.1 Box model experiments

A box model comparison study was performed with the different isoprene schemes to establish any inherent differences in the schemes that do not arise from the complexity present in a global 3-D model. This also allows us to compare the reduced





ACPD
14, 22385–22435, 2014

schemes with a more complex scheme, the MCMv3.2 (Jenkin et al., 1997; Archibald et al., 2010b), which is too complex to put into a global 3-D chemistry–climate model. The detailed nature of the MCM lends itself to being a benchmark mechanism against which the others can be compared (e.g. Archibald et al., 2010b). However, the MCM still contains approximations; e.g. many of the rate constants are inferred from other reactions using structure reactivity relationships (SARs, e.g. Kwok and Atkinson, 1995; McGillen et al., 2011), and only four of the six $ISO_2$ isomers are included.

For our box model comparison, the Kinetic PreProcessor (KPP) solver (Sandu and Sander, 2006) was used, with a model timestep of 20 min. The model was set up so that different emissions of $NO_x$ and isoprene were input, allowing us to study how the mechanisms compared over a wide range of $NO_x$-to-isoprene ratios. $NO_x$ emissions between 0.001 and 0.5 mg N $m^{-2}$ $h^{-1}$ and isoprene emissions between 0.0001 and 6 mg C $m^{-2}$ $h^{-1}$ were used, with emission rates being constant for the duration of a given model run. Atmospheric pressure ($1 \times 10^5$ Pa) and temperature (298 K) were kept constant, and the amount of light varied through the day as in a gridcell at 14° latitude on Julian day 172 (solar declination angle = 23.44°). The model was initialised with 30 ppb $O_3$, 1820 ppb $CH_4$, 102 ppb CO, and run with a fixed amount of $H_2O$ (0.01 %). All runs lasted three days, and in all cases the maximum $O_3$ value on the third day was compared. It should be noted that this was not long enough for the system to reach steady state. The box model does not include any advection or deposition processes, and as such $O_3$ values are likely to be higher than those measured in the field or calculated in UM-UKCA. The MCM photolysis scheme was used for all schemes. The results of the box model comparison are given in Sect. 3.

### 2.2.2 Global perturbation experiments

To investigate the influence of variations in the isoprene mechanism on potential changes in tropospheric $O_3$ over the 21st century, a global chemistry–climate model (the UK Met Office Unified Model coupled to the UK Chemistry and Aerosol model,





ACPD
14, 22385–22435, 2014



CC BY

UM-UKCA) was used, as specified in Squire et al. (2014). For each mechanism investigated, a present day (2000) integration was conducted, following the model setup described for the BASE run in Squire et al. (2014). Then for each mechanism four future (2095) integrations were conducted to investigate (1) CC, climate change only, (2) IC, isoprene emission change with climate, (3) AC, anthropogenic emission change, and (4) LC, land use change, with each integration set up as described in Squire et al. (2014). The effect of mechanistic changes on the $O_3$ response to including the $CO_2$-inhibition of isoprene emissions was not investigated in this study.

For CC all parameters, including isoprene emissions, remained as in the present day BASE run except sea surface temperatures, sea ice concentrations and greenhouse gas concentrations. In IC, isoprene emissions were allowed to vary with a scenario of future climate change. This led globally to higher isoprene emissions (545 $Tg\,C\,yr^{-1}$) than in the BASE run (467 $Tg\,C\,yr^{-1}$), largely due to the effect of extended $CO_2$-fertilisation of the biosphere under the elevated $CO_2$ levels. AC was characterised by stringent emission cuts across much of the northern hemispheric developed regions, leading to lower $NO_x$ levels there. For LC we used a scenario of future cropland expansion, which is dominated by the replacement of tropical broadleaf trees with crops (see Squire et al. (2014) for details). As our crops emit less isoprene than broadleaf trees (Guenther et al., 2006; Lathiere et al., 2010), this causes a decrease in isoprene emissions (190 $Tg\,C\,yr^{-1}$ globally).

## 3 Mechanism intercomparison with a box model

As outlined in Sect. 2.2.1, a comparison of the reduced isoprene schemes with the MCM was conducted using a box model. For each mechanism, box model runs were performed at a series of different $NO_x$ and isoprene emission rates, so that an $O_3$ isopleth plot could be constructed, similar to those found in Dodge (1977) and Sillman and He (2002). With the MCM (Fig. 1), when both $NO_x$ and isoprene are low, $O_3$ stays around the initial concentration (30 ppb). As emission rates of both $O_3$ precursors in-





ACPD
14, 22385–22435, 2014



CC BY

crease, $O_3$ increases reaching a maximum of 140–160 ppb at the highest emission rates used (0.5 mg N $m^{-2}$ $h^{-1}$ of $NO_x$ and 6 mg C $m^{-2}$ $h^{-1}$ of isoprene – top right-hand corner). When isoprene emissions are low and $NO_x$ emissions are high (top left-hand corner) net $O_3$ destruction occurs that is consistent with high nitric acid formation ($O_x$ loss via $NO_2 + OH$). When isoprene emissions are high and $NO_x$ emissions are low, as in a tropical rainforest, (lower right-hand corner) net $O_3$ destruction occurs as is consistent with high levels of isoprene ozonolysis.

Figure 2 shows the bias in the isopleth plot compared to the MCM (Fig. 1) for the four reduced mechanisms as a percentage difference. For CheT (Fig. 2a), the bias is generally within ±20 % of the MCM, however at high $NO_x$ and isoprene emissions the bias is higher, with CheT calculating up to nearly 40 % less $O_3$ than the MCM. Overall the mean bias (MB) is −5.7 %, indicating a weak negative bias compared to the MCM. This result is consistent with the work of Archibald et al. (2010b) who showed that the CheT scheme (UKCA in their runs) simulated lower levels of $O_3$ than the MCMv3.1.

In CheT2 (Fig. 2b) the low bias at high $O_3$ precursor emissions is much less pronounced than it was in CheT, being within ±20 % of the MCM. This is consistent with the lower rate of MPAN formation in CheT2 compared to CheT, meaning more $NO_x$ is available for $O_3$ formation. CheT2 however has a high bias compared to the MCM at low $NO_x$ and high isoprene emissions, calculating up to ∼ 40 % more $O_3$ in this regime. This could be related to the additional $HO_x$ regeneration pathway present in CheT2 (the Peeters mechanism, Peeters et al., 2009), which is not included in the MCMv3.2. This finding is consistent with the enhanced $O_3$ seen in Archibald et al. (2011) when CheT (UKCA in their work) was run with inclusion of the Peeters mechanism. Overall the MB of CheT2 with respect to the MCM is lower (−1 %) than for CheT (−5.7 %).

For AQUM (Fig. 2c) there is a large negative MB (−25 %) compared to the MCM. The main contribution to this bias occurs under high $NO_x$ and low isoprene conditions. Conversely, under low $NO_x$, high isoprene conditions, AQUM is biased high by ∼ 20 %.

LLSF shows the highest biases in $O_3$ compared to the MCM (Fig. 2d). At low $NO_x$ high isoprene emissions, LLSF is biased high by up to ∼ 80 %. Under high isoprene





ACPD
14, 22385–22435, 2014



CC BY

emissions, mixing ratios of peroxy radicals are high, leading to substantial peroxy radical loss via peroxy-radical-peroxy-radical reactions (e.g. $RO_2 + HO_2$). $O_3$ is higher under these conditions in LLSF, in which all isoprene-derived peroxy radicals are represented as methyl peroxy radicals ($MeO_2$), as the reaction between $MeO_2$ and $HO_2$ is slower than for the major isoprene-derived peroxy-radicals in the MCM. At high $NO_x$ low isoprene emissions, LLSF is biased low by ∼ 40 %. With LLSF, the low bias at low isoprene emissions and high bias at high isoprene emissions largely cancel each other out, leading to a small MB (−2.6 %).

Overall, CheT2 shows the least bias compared to the MCM (MB of −1 %), except for at high isoprene low $NO_x$ conditions. A more in depth analysis and discussion of the differences between the reduced mechanisms themselves is undertaken in the following sections, when we bring in the results from the global model.

## 4 Present day mechanism intercomparison with a global model

Using the four reduced schemes, global simulations of the present day atmosphere were conducted. Figure 3a shows near surface $O_3$ for the present day using the CheT isoprene scheme. Figure 3b–d illustrates the change in this $O_3$ caused by the use of different isoprene chemical schemes. All schemes simulate a present day tropospheric $O_3$ burden that is within one standard deviation of the model ensemble mean from the ACCENT study (344 ± 39 Tg) (Stevenson et al., 2006). As may be expected from a comparison of isoprene chemical mechanisms, the largest differences between the schemes occur where isoprene emissions are highest (tropical regions and the southeast USA). In these regions (mean isoprene emissions $> 0.1\,mg\,C\,m^{-2}\,h^{-1}$) the mean surface $O_3$ for CheT is 41 ppb, whilst for AQUM and LLSF the values are higher (46 ppb (+11 %) and 50 ppb (+18 %) respectively). In some places (e.g. Amazonia, Central Africa) this equates to surface $O_3$ that is at least 10 ppb higher than with CheT. By comparison, surface $O_3$ in CheT2 is very similar to that of CheT, even in the high isoprene emitting regions.





ACPD
14, 22385–22435, 2014



CC BY

The regions of high isoprene emissions, where the largest differences between the mechanisms are calculated, are generally situated away from areas of intense anthropogenic activity. As a result, these areas tend to have low $NO_x$ emissions. To understand the changes occurring in this low-$NO_x$ high-isoprene regime, Table 3 gives the mean $O_x$ budget fluxes for near surface (below 720 m) gridcells with monthly mean $NO_x$ emissions less than 0.03 mg N $m^{-2}$ $h^{-1}$ and monthly mean isoprene emissions greater than 0.1 mg C $m^{-2}$ $h^{-1}$ (roughly matching the bottom right-hand quarter of Fig. 1). Here we define $O_x$ as $O^3P + O^1D + O_3 + 2 \times NO_3 + NO_2 + 3\times$ dinitrogen pentoxide ($N_2O_5$) + nitric acid ($HNO_3$) + peroxynitric acid ($HNO_4$) + PAN + peroxypropionyl nitrate (PPAN) + MPAN. Figure 4 shows geographical locations of those gridcells included in this emissions regime, and also indicates how many months per year each gridcell was included.

From the budget terms in Table 3 for the BASE integrations, total mean $O_x$ production varies across the schemes from 74 mol $gc^{-1}$ $s^{-1}$ (here gc = gridcell) (CheT and CheT2) to 200 mol $gc^{-1}$ $s^{-1}$ (LLSF). The majority of this variance is due to differences in the peroxy-radical + NO reactions ($HO_2$ + NO, $MeO_2$ + NO and other peroxy-radicals ($RO_2$) + NO). In CheT, CheT2 and AQUM, $RO_2$ is primarily $ISO_2$, $MACRO_2$ (see Table 1 for definitions) and the peroxy acetyl radical ($MeCO_3$).

In all schemes, the oxidation of isoprene by OH is a source of peroxy radicals. In CheT, CheT2 and AQUM, the initial isoprene + OH reaction leads exclusively to the production of $ISO_2$, whilst for LLSF $MeO_2$ is produced instead. Both $MeO_2$ and $ISO_2$ may react with NO producing $O_x$ (propagation), or with other peroxy radicals producing peroxides (termination). $k_{ISO_2+HO_2}$ (similar in all schemes that include $ISO_2$) is three times higher than $k_{MeO_2+HO_2}$ (identical in all schemes), and $k_{MeO_2+NO}$ (identical in all schemes) is two times higher than $k_{ISO_2+NO}$ (similar in all schemes that include $ISO_2$). This suggests that the scheme that produces the largest fraction of $MeO_2$ from isoprene oxidation (LLSF) should also show the highest total $RO_2$ + NO flux and consequently highest $O_3$ levels, exactly as calculated (see Fig. 3d).





ACPD
14, 22385–22435, 2014



CC BY

In CheT, CheT2 and AQUM, once $ISO_2$ is formed, it may be further oxidised to produce second generation peroxy radicals such as $MACRO_2$. In AQUM, reactions of $ISO_2$ and $MACRO_2$ with NO lead to greater production of $O_3$, as evident from the higher mean $RO_2 + NO$ flux (Table 3): 51 mol gc$^{-1}$ s$^{-1}$ (AQUM), 31 mol gc$^{-1}$ s$^{-1}$ (CheT), 29 mol gc$^{-1}$ s$^{-1}$ (CheT2). The reason for this is the inclusion in CheT and CheT2 of competing peroxy radical + NO reaction channels that do not lead to $O_3$ formation. AQUM does not include the isoprene nitrate formation pathway from $ISO_2$, which accounts for 4.4 % and 10 % of the total $ISO_2$ + NO flux in CheT and CheT2 respectively (Jenkin, 2012). Additionally, AQUM does not include MPAN formation from $MACRO_2 + NO$, which contributes to a lower mean $MACRO_2 + NO \rightarrow NO_2$ flux in CheT and CheT2 compared to AQUM: 7.0 mol gc$^{-1}$ s$^{-1}$ (CheT), 6.7 mol gc$^{-1}$ s$^{-1}$ (CheT2) and 12 mol gc$^{-1}$ s$^{-1}$ (AQUM).

Figure 5 shows total peroxyacyl nitrates (ΣPAN = PAN + MPAN + PPAN) near the surface in (a) CheT and (b–d) the difference between CheT and the other schemes. Figure 5d shows that compared to CheT, there is much less ΣPAN in LLSF (the ΣPAN tropospheric burden in LLSF is 1.49 Tg compared to 3.57 Tg in CheT). This follows since in LLSF no ΣPAN precursor radicals ($MeCO_3$ nor $MACRO_2$) are produced from isoprene oxidation. As PANs are a source of $O_x$ to remote regions, the low ΣPAN in LLSF is likely the cause of the low $O_3$ compared to CheT over the remote Tropical oceans (a mean reduction of 10 % between ±20° lat, Fig. 3d). Another consequence of reduced PAN formation, is that more $NO_x$ stays close to the isoprene source region, which will contribute to the higher total $RO_2 + NO$ flux, and hence higher $O_3$, in these regions in LLSF.

Figure 5b indicates that ΣPAN in CheT2 is marginally lower than in CheT (the ΣPAN tropospheric burden is about 6 % lower). The cause of this is the fact that the MPAN production rate in CheT2 is set to be 10 % of that in CheT. The CheT2 rate is the value we would recommend, as it has been adjusted to take account of the fact that in UKCA, the species $MACRO_2$ represents a set of peroxy radicals, not just the MPAN precursor methacrolyl peroxy radical (Jenkin, 2012).





ACPD
14, 22385–22435, 2014



CC BY

Figure 5c shows that ΣPAN in AQUM is again marginally lower than in CheT (tropospheric ΣPAN burden is 7 % lower), this time due to the total absence of MPAN formation. However, the difference is small owing to the fact that in AQUM PAN production is higher, a result of higher production of the PAN precursor radical $MeCO_3$ from isoprene oxidation. The mean mixing ratio of $MeCO_3$ is 29 % higher than the average of that in CheT and CheT2. Possible additional sources of $MeCO_3$ in AQUM are the higher yield of methyglyoxal (MGLY), which rapidly reacts to form $MeCO_3$ (CheT and CheT2 = 16 Tg MGLY $yr^{-1}$, AQUM = 40 Tg MGLY $yr^{-1}$). The higher yield of the $MeCO_3$ peroxy radical would also account for a fraction of the higher $RO_2$ + NO flux, and hence higher $O_3$ in AQUM.

Extending the comparison to the wider troposphere, Table 4 gives the summed total $O_x$ budget fluxes for the different schemes up to the tropopause. To complement this, Fig. 6 shows the zonal mean ozone for the entire troposphere. The tropopause is shown by the black line. It is immediately apparent that the differences in $O_3$ at the surface are not representative of the net effect on $O_3$ over the entire troposphere. Whilst the $O_3$ burdens of CheT and CheT2 are very similar (379 and 380 Tg respectively), AQUM has a lower burden (374 Tg) and LLSF lower still (360 Tg). This is consistent with the zonal difference plots (Fig. 6b–d), which show that away from the surface, both AQUM and LLSF give lower $O_3$ than CheT, most notably in the tropical tropopause region.

Although the highest total tropospheric net chemical production is calculated for LLSF, (499 Tg $yr^{-1}$), overall the $O_3$ burden is lower due to the higher rate of dry deposition (1180 Tg $yr^{-1}$) compared to CheT (1155 Tg $yr^{-1}$) and CheT2 (1154 Tg $yr^{-1}$) (see Fig. 7). The rate of dry deposition in AQUM is also high (1191 Tg $yr^{-1}$) (Fig. 7c). In UM-UKCA dry deposition only occurs at the surface and is highest over forested regions. As AQUM and LLSF both produce higher $O_3$ near the surface and notably over forested regions (high isoprene emitting regions), dry deposition is likely to be higher. This is indeed the case as illustrated by Fig. 7, which shows much higher $O_3$ dry deposition fluxes over forested regions (e.g. Amazonia, central Africa) in AQUM and LLSF compared to CheT. CheT and CheT2 have higher rates of ΣPAN formation,





ACPD
14, 22385–22435, 2014



CC BY

leading to more $O_3$ production away from forested regions and the surface in general, thus resulting in lower $O_3$ dry deposition and higher overall tropospheric $O_3$ burdens.

Although tropospheric $O_3$ varies little between CheT and CheT2 (Figs. 3 and 6), there are larger changes in other key oxidants, notably OH. Due to the inclusion of additional $HO_x$ regeneration pathways within the isoprene oxidation mechanism of CheT2 (namely the Peeters mechanism, Peeters et al., 2009), one would expect CheT2 to show higher levels of OH over high isoprene-emitting regions. Figure 8 shows that OH in CheT2 is indeed higher than in CheT over the main isoprene-emitting regions, with maximum increases of approximately 50 %. Warwick et al. (2013) also calculated that including the Peeters mechanism in UM-UKCA gave higher OH, improving agreement between modelled and measured values.

## 5 Future perturbation experiments

In the previous section, we compared the different isoprene mechanisms under present day conditions. In this section we examine how the mechanisms compare in the context of the future climate change (Sect. 5.1) and future isoprene emission change (Sect. 5.2) perturbation experiments described in Sect. 2.2.2.

### 5.1 Climate change

Figure 9a shows the change in near surface $O_3$ caused by our climate change scenario (CC) using the CheT scheme, as in Squire et al. (2014). Figure 9b–d shows the effect of CC using instead the CheT2, AQUM and LLSF isoprene schemes respectively. The general pattern of near surface $O_3$ changes is similar in all schemes. There are reductions over the oceans due to increased water vapour and subsequent loss of $O_3$ via increased $O^1D + H_2O$. Over land where $O_3$ production dominates (e.g. polluted northern-hemispheric regions), near surface $O_3$ increases as the flux through $O_x$ producing reactions usually increases with temperature. In regions with high isoprene emissions such





ACPD
14, 22385–22435, 2014



CC BY

as the Tropics, $O_3$ also tends to increase, due to changes in PAN. PAN decomposition exhibits a strong temperature dependence, such that under the higher temperatures of climate change PAN decomposes faster, thus more $NO_x$ will be present near the isoprene emission source. As a result, the mean $\Sigma RO_2$ $(= HO_2 + MeO_2 + RO_2) + NO$ flux increases in these regions (see CC entries in Table 3) (AQUM = +15 mol gc$^{-1}$ s$^{-1}$, CheT = +10 mol gc$^{-1}$ s$^{-1}$, CheT2 = +9.3 mol gc$^{-1}$ s$^{-1}$) leading to higher $O_3$ near the isoprene emission source.

Unlike with the other schemes, with LLSF in high isoprene low $NO_x$ regions, $O_3$ decreases. This is because firstly LLSF produces very little PAN compared to the other schemes (see Sect. 4), so no increase in $NO_x$ is calculated as would occur with increased PAN decomposition. The fact that $O_3$ actually decreases is due to the negative temperature dependence of $k_{C_5H_8+OH}$. The flux through this reaction under climate change decreases by ~ 20 % in all schemes, leading to associated increases in OH. Lower isoprene oxidation rates lead to a lower rate of peroxy-radical production, and thus the $HO_2 + NO$ and $MeO_2 + NO$ reaction fluxes decrease in LLSF (−1.8 mol gc$^{-1}$ s$^{-1}$ and −3.2 mol gc$^{-1}$ s$^{-1}$ respectively, Table 3). In schemes other than LLSF, this effect is masked by the large increase in $NO_x$ from increased PAN decomposition. Despite large changes in tropospheric net chemical production due to climate change, the tropospheric $O_3$ burdens in the CC experiment remain unaltered (Table 3).

We also explored how ozone changes with our future anthropogenic emission scenario (AC, not shown). This scenario is characterised by large reductions in $NO_x$ emissions over the USA, Europe and Japan. The $O_3$ response was remarkably similar for all the different isoprene mechanisms, presumably because the largest changes in anthropogenic emissions occur away from regions of high isoprene emissions. We conclude that the $O_3$-$NO_x$ response in these regions is controlled largely by the simple $NO_x$-$HO_x$ chemistry which is the same in all chemistry schemes.





ACPD
14, 22385–22435, 2014



CC BY

## 5.2 Isoprene emission change

In this section we examine the results of the two isoprene emission change experiments; IC – the change in isoprene emissions with climate, and LC – the change in isoprene emissions with land use.

Figures 10 and 11 show the changes in surface $O_3$ that occur for each of the different isoprene chemical mechanisms in the IC and LC experiments respectively. In both cases, the isoprene mechanism sensitivity is more pronounced than for the CC experiment (Sect. 5.1), which may be anticipated given the perturbations in IC and LC specifically involve isoprene. On the scale of the whole troposphere, the $O_3$ burden is enhanced in IC and reduced in LC for all schemes (Table 4). This is expected as in IC ultimately there is more $O_3$ precursor and in LC there is less.

In the next three sub-sections, we will analyse the $O_3$ trends in Figs. 10 and 11 using the corresponding $O_x$ budget terms in Tables. 3 and 5. This will be done for each distinct $O_x$ production regime; Sect. 5.2.2 – $NO_x$-limited regions where isoprene emissions increase, Sect. 5.2.3 – $NO_x$-limited regions where isoprene emissions decrease, and Sect. 5.2.4 – VOC-limited regions where isoprene emissions increase. In the next section (Sect. 5.2.1) we discuss precisely how each of these regimes is defined.

### 5.2.1 Defining distinct $O_x$ production regimes

In the IC experiment a mean global increase in isoprene emissions ($+78\,\mathrm{Tg\,C\,yr^{-1}}$) is calculated. Within the high isoprene-emitting regions, there are three distinct regimes of change, which we will denote as IC regions 1, 2 and 3 (ICr1, ICr2 and ICr3). Each regime is defined on a per-month-per-gridcell basis as follows:

1. ICr1 = months when isoprene emissions in a gridcell increase by more than 0.05 Tg and the environment is $NO_x$-limited.

2. ICr2 = months when isoprene emissions in a gridcell decrease by more than 0.05 Tg and the environment is $NO_x$-limited.





ACPD
14, 22385–22435, 2014

3. ICr3 = months when isoprene emissions in a gridcell increase by more than 0.005 Tg and the environment is VOC-limited.

The isoprene emission change criteria is an order of magnitude smaller for ICr3 than for ICr1 or ICr2, owing to the greater sensitivity of increasing isoprene emissions in a VOC-limited environment compared to a $NO_x$-limited environment. Here we define VOC-limited as where the ratio of $L_N$ (loss of radicals from reactions with NO and $NO_2$) to Q (the sum of all radical sinks) is more than 0.5 (Kleinman et al., 1997; Wiedinmyer et al., 2006). $NO_x$-limited is defined as where $L_N/Q$ is less than 0.5 (Kleinman et al., 1997; Wiedinmyer et al., 2006). To ensure that each regime includes the same gridcells in CheT, CheT2, AQUM and LLSF, $L_N/Q$ values from CheT were used in all cases. The geographical location of those gridcells included in each regime are shown Fig. 12, indicating also how many months per year each gridcell was included. Table 5 gives mean $O_x$ budget fluxes for these three regimes, which will be discussed in Sects. 5.2.2–5.2.4.

In LC the pattern of change in all high isoprene-emitting regions is the same as that of ICr2; reductions in isoprene-emissions ($-190\,\mathrm{Tg\,C\,yr^{-1}}$ globally) in a $NO_x$-limited environment. As such, LC and ICr2 will be discussed together. Note that those high isoprene-emitting regions that were VOC-limited in IC (ICr3, e.g. southeastern USA) are $NO_x$-limited in LC owing to the inclusion of an anthropogenic emission scenario of large northern hemispheric $NO_x$ emission reductions. The mean $O_x$ budget terms for LC are given in Table 3 calculated using the same gridcells as the other budgets in this table (see Fig. 4).

### 5.2.2 $NO_x$-limited regions where isoprene emissions increase (ICr1)

In ICr1 where isoprene emissions increase in a $NO_x$-limited environment, both total chemical $O_x$ production and total chemical $O_x$ loss increase in all schemes, owing to greater $O_3$ precursor emissions. Changes in $O_x$ loss are similar in all schemes, being driven largely by an increase in isoprene ozonolysis (in the range





ACPD
14, 22385–22435, 2014

+21 to +27 mol gc$^{-1}$ s$^{-1}$ across the schemes). On the other hand, total $O_x$ production varies considerably between schemes, from ∼ +1 mol gc$^{-1}$ s$^{-1}$ in CheT and CheT2, to +90 mol gc$^{-1}$ s$^{-1}$ in LLSF. The overall result is a decrease in net $O_x$ production for CheT and CheT2 (each −16 mol gc$^{-1}$ s$^{-1}$), close to no net change in AQUM, and a net increase in LLSF (+50 mol gc$^{-1}$ s$^{-1}$). As explained in Sect. 4, the primary peroxy radical produced from isoprene oxidation in LLSF is $MeO_2$, whilst in the other schemes it is $ISO_2$ and $MACRO_2$. $MeO_2$ has a higher propensity for reaction with NO than $ISO_2$ or $MACRO_2$, thus an increase in isoprene emissions (as in ICr1) will increase the total $RO_2$ + NO flux by a greater amount in LLSF than in the other schemes. Note that the MPAN and isoprene-nitrate formation pathways that compete directly with $O_x$ production from isoprene-derived peroxy radicals in CheT and CheT2, are not included in AQUM. Accordingly, increasing isoprene emissions in AQUM leads to a larger increase in the $\Sigma RO_2$ + NO flux than in CheT or CheT2.

#### 5.2.3 $NO_x$-limited regions where isoprene emissions decrease (LC and ICr2)

In LC and ICr2 where isoprene emissions are reduced in a $NO_x$-limited environment, the opposite trend is calculated compared to ICr1. Both $O_x$ loss and production decrease due to lower levels of $O_3$ precursor emissions. As with ICr1, the change in $O_x$ loss is similar in all schemes, being driven by reductions in isoprene ozonolysis (on average −11 mol gc$^{-1}$ s$^{-1}$ (LC) and −15 mol gc$^{-1}$ s$^{-1}$ (ICr2) (∼ −50 %)). Again, on the other hand, total $O_x$ production varies considerably between schemes (from −1.7 mol gc$^{-1}$ s$^{-1}$ (LC) and ∼ −10 mol gc$^{-1}$ s$^{-1}$ (ICr2) in CheT and CheT2, to −45 mol gc$^{-1}$ s$^{-1}$ (LC) and −149 mol gc$^{-1}$ s$^{-1}$ (ICr2) in LLSF). The reduction in isoprene emissions causes a proportionally larger decrease in $\Sigma RO_2$ + NO for LLSF compared to the other schemes due to the preferential formation of $MeO_2$ from isoprene oxidation compared to other peroxy radicals. This leads to a large reduction in net $O_x$ formation in LLSF (−24 mol gc$^{-1}$ s$^{-1}$ (LC), −113 mol gc$^{-1}$ s$^{-1}$ (ICr2)). For AQUM, the lower rate of formation of $NO_x$ reservoir species compared to CheT or CheT2 leads to a greater





ACPD
14, 22385–22435, 2014



CC BY

reduction in $\Sigma RO_2 + NO$, overall leading to a moderate reduction in net $O_x$ production ($-4.0\,mol\,gc^{-1}\,s^{-1}$ (LC), $-53\,mol\,gc^{-1}\,s^{-1}$ (ICr2)). Finally, for CheT and CheT2, the increase in $O_3$ caused by the reduction in isoprene ozonolysis outweighs reductions in $O_3$ caused by reductions in $\Sigma RO_2 + NO$, leading overall to increases in net $O_x$ production (each $+6.7\,mol\,gc^{-1}\,s^{-1}$ (LC), $+1.4\,mol\,gc^{-1}\,s^{-1}$ (ICr2, CheT2)) or close to no change ($-0.4\,mol\,gc^{-1}\,s^{-1}$ (ICr2, CheT)).

#### 5.2.4 VOC-limited regions where isoprene emissions increase (ICr3)

For ICr3, where isoprene emissions increase in a VOC-limited environment, all schemes show the same trend of increased near surface $O_3$. In such an environment, the effect of adding isoprene favours $O_3$ production to a far greater extent than $O_3$ loss, owing to the availability of $NO_x$. The result is that in all schemes, even CheT and CheT2 that have a lower overall propensity for $O_x$ production, net $O_x$ production increases ($+25\,mol\,gc^{-1}\,s^{-1}$ (CheT), $+26\,mol\,gc^{-1}\,s^{-1}$ (CheT2), $+46\,mol\,gc^{-1}\,s^{-1}$ (AQUM), $+47\,mol\,gc^{-1}\,s^{-1}$ (LLSF), Table 5).

## 6 A comparison of $O_3$ sensitivity to precursor emissions in global and box models

Figure 13 shows $O_3$ isopleths as a function of $NO_x$ and isoprene emission, similar to that in Fig. 1, but for the reduced schemes and in this case using $O_3$ mixing ratio data from the global UM-UKCA simulations. Data from all of the experiments discussed in Sect. 5 were included in Fig. 13 to maximise the $NO_x$-isoprene emission space that was covered (the exact same emission values were earlier used to produce Figs. 1 and 2). The arrows in Fig. 13 indicate the mean emission of $NO_x$ and isoprene in the Amazon region, before and after land use change (i.e. those emissions used in the AC and LC integrations). It becomes clear that for CheT and CheT2, the gradient of the





ACPD
14, 22385–22435, 2014



CC BY

contours is such that $O_3$ increases with the isoprene emission change, but for the other two schemes, $O_3$ decreases. This is consistent with the picture presented in Fig. 11.

Comparing Fig. 13 to Figs. 1 and 2, the principle features of the isopleths derived from the global model are captured well by the box model simulations. This includes resolution of the differences between the schemes, such as the higher $O_3$ in LLSF and AQUM at high isoprene emissions compared to CheT and CheT2. In fact, compared to the global model, the box model simulations tend to accentuate the chemical differences between the schemes. With the isopleths derived from the global model simulations, the effects of advection and deposition somewhat buffer those chemical differences, leading to a narrower range of $O_3$ mixing ratios and more similar isopleths. Consequently, the $O_3$ levels reached in the global simulations (less than 70 ppb) are generally lower than in the box model (approaching 170 ppb). The high level of qualitative agreement between the isopleths derived from the box model and global model suggests that the method of constructing such isopleths with the far less computationally expensive box models is a convenient way to quickly and accurately assess differences between chemical mechanisms. The fact that Figs. 1, 2 and 13 show good agreement, gives us confidence that the comparison to a near-explicit mechanism (the MCM), that out of computational necessity had to be performed with a box model, would also be relevant for global model experiments.

## 7 Conclusions

In this work we have examined the effect of using various reduced isoprene chemical mechanisms, all of which are currently used in ESMs, on tropospheric $O_3$ and on its sensitivity to climate change (CC), isoprene emission changes with climate (IC), anthropogenic emission changes (AC), and land use change (LC). Between the CheT and CheT2 schemes, there is no significant difference in near-surface $O_3$, though OH is higher in isoprene-emitting regions in CheT2 due to the inclusion of additional $HO_x$ regeneration pathways from isoprene oxidation. For the BASE run, in the major iso-





ACPD
14, 22385–22435, 2014

prene emitting regions AQUM and LLSF give $O_3$ levels that are at least 10 ppb higher than with the other schemes. This is due to differences in the speciation of peroxy-radicals produced by the schemes. LLSF produces a large yield of $MeO_2$ that rapidly reacts with NO to form $O_3$. The other schemes produce $ISO_2$, which has a higher rate of radical termination than $MeO_2$, thus leading to less $O_3$ formation. AQUM produces more $O_3$ than CheT and CheT2 because the scheme makes less ISON and no MPAN, both important $NO_x$ sinks near the isoprene emission source.

Turning to the future perturbation experiments, in CC the $O_3$-climate change sensitivity is similar in all schemes, though LLSF responds differently over the Amazon, due to the fact that no PANs are produced in significant amounts. In the anthropogenic emission change experiment (AC), which is characterised by large $NO_x$ emission reductions in the northern hemisphere, all mechanisms respond in a similar way. This suggests that the $O_3$-$NO_x$ response is driven largely by the simple $NO_x$-$HO_x$-alkane chemistry, which is the same for all schemes.

With the isoprene-emission change experiments (IC and LC), there are changes in both isoprene ozonolysis ($O_x$ loss) and the $\Sigma RO_2 + NO$ flux ($O_x$ production). For the land use change experiment (LC), isoprene emissions decrease leading to a reduction in both processes. The ozonolysis changes are the same in all schemes, but the $RO_2 + NO$ reductions differ widely between schemes. For LLSF reductions are largest owing to the high yield of $MeO_2$, which favours reaction with NO compared to higher isoprene-derived peroxy radicals ($ISO_2$ and $MACRO_2$). These are produced by the other schemes, leading overall to a smaller reduction in $RO_2 + NO$. In LLSF and AQUM the reduction in $RO_2 + NO$ is sufficient to cause a net decrease in near surface $O_3$ in response to land use, however this is not the case for CheT and CheT2, due to the formation of MPAN and additional ISON. For IC (increase in emissions), the opposite trends are calculated, though AQUM is in closer agreement with CheT and CheT2. This is most likely due to smaller net isoprene emission changes in IC compared to LC. In IC where isoprene emissions increase under VOC-limited conditions (e.g. southeast





ACPD
14, 22385–22435, 2014



CC BY

USA), all schemes show a net increase in near surface $O_3$ owing to the fact that an increase in isoprene emissions strongly favours $O_x$ production under such conditions.

Squire et al. (2014) used the CheT scheme and found that the calculated increases in $O_3$ due to cropland expansion (LC) were not great enough to cause a significant increase in $O_3$-induced vegetation damage. CheT2 calculates very similar $O_3$ changes and both AQUM and LLSF calculate net decreases in $O_3$ with cropland expansion, suggesting that this conclusion would not change with the use of these schemes, and further calculations (not shown) demonstrate this to be the case.

By using the emissions and $O_3$ data from all of the global model experiments, we were able to construct $O_3$ isopleths in terms of $NO_x$ and isoprene emissions. These isopleths were useful in explaining the global model response to isoprene emission changes. Using these same $O_3$ precursor emissions, we also constructed $O_3$ isopleths using a box model. We find there to be good qualitative agreement between those isopleths derived from the global model and those from the box model. This suggests that comparing chemical mechanisms with a box model in this framework is a computationally cheap yet accurate tool for assessing mechanistic performance in complex global models. Furthermore, the good agreement between box and global models gives us confidence that the box model comparison to a near-explicit mechanism carries weight in the global model experiments. Here we have shown that the magnitude and even the sign of the $O_3$ response is affected by the choice of reduced isoprene mechanism. This suggests that in such perturbation experiments how isoprene chemistry is parameterised is an important consideration and certainly not something to be overlooked.

*Acknowledgements.* We would like to acknowledge funding from the National Environmental Research Council (NERC), the National Centre for Atmospheric Science (NCAS) and the European Research Council (ERC) under project no 267760 – ACCI. A. T. A. would like to acknowledge funding from the Herschel Smith Fund.





ACPD
14, 22385–22435, 2014



CC BY

## References


Archibald, A. T., Cooke, M. C., Utembe, S. R., Shallcross, D. E., Derwent, R. G., and Jenkin, M. E.: Impacts of mechanistic changes on $HO_x$ formation and recycling in the oxidation of isoprene, Atmos. Chem. Phys., 10, 8097–8118, doi:10.5194/acp-10-8097-2010, 2010a. 22389, 22391

Archibald, A. T., Jenkin, M. E., and Shallcross, D. E.: An isoprene mechanism intercomparison, Atmos. Environ., 44, 5356–5364, doi:10.1016/j.atmosenv.2009.09.016, 2010b. 22387, 22393, 22395

Archibald, A. T., Levine, J. G., Abraham, N. L., Cooke, M. C., Edwards, P. M., Heard, D. E., Jenkin, M. E., Karunaharan, A., Pike, R. C., Monks, P. S., Shallcross, D. E., Telford, P. J., Whalley, L. K., and Pyle, J. A.: Impacts of $HO_x$ regeneration and recycling in the oxidation of isoprene: consequences for the composition of past, present and future atmospheres, Geophys. Res. Lett., 38, L05804, doi:10.1029/2010GL046520, 2011. 22395

Aumont, B., Szopa, S., and Madronich, S.: Modelling the evolution of organic carbon during its gas-phase tropospheric oxidation: development of an explicit model based on a self generating approach, Atmos. Chem. Phys., 5, 2497–2517, doi:10.5194/acp-5-2497-2005, 2005. 22387

Cameron-Smith, P., Prather, M. J., Lamarque, J., Hess, P. G., Connell, P. S., Bergmann, D. J., and Vitt, F. M.: The super-fast chemistry mechanism for IPCC AR5 simulations with CCSM, in: American Geophysical Union, Fall Meeting, 18 December 2009, San Francisco, A54A-08, 2009. 22392

Chameides, W., Lindsay, R., Richardson, J., and Kiang, C.: The role of biogenic hydrocarbons in urban photochemical smog – Atlanta as a case-study, Science, 241, 1473–1475, doi:10.1126/science.3420404, 1988. 22387

Dodge, M.: Combined use of modeling techniques and smog chamber data to derive ozone-precursor relationships, in: Proceedings of the International Conference on Photochemical Oxidant Pollution and its Control, US Environmental Protection Agency, Research Triangle Park, NC, USA, 881–889, 1977. 22394

Farmer, D. K. and Cohen, R. C.: Observations of $HNO_3$, ΣAN, ΣPN and $NO_2$ fluxes: evidence for rapid $HO_x$ chemistry within a pine forest canopy, Atmos. Chem. Phys., 8, 3899–3917, doi:10.5194/acp-8-3899-2008, 2008. 22390






ACPD
14, 22385–22435, 2014

Fiore, A. M., Naik, V., Spracklen, D. V., Steiner, A., Unger, N., Prather, M., Bergmann, D., Cameron-Smith, P. J., Cionni, I., Collins, W. J., Dalsoren, S., Eyring, V., Folberth, G. A., Ginoux, P., Horowitz, L. W., Josse, B., Lamarque, J.-F., MacKenzie, I. A., Nagashima, T., O'Connor, F. M., Righi, M., Rumbold, S. T., Shindell, D. T., Skeie, R. B., Sudo, K., Szopa, S., Takemura, T., and Zeng, G.: Global air quality and climate, Chem. Soc. Rev., 41, 6663–6683, doi:10.1039/C2CS35095E, 2012. 22389

Fuchs, H., Bohn, B., Hofzumahaus, A., Holland, F., Lu, K. D., Nehr, S., Rohrer, F., and Wahner, A.: Detection of $HO_2$ by laser-induced fluorescence: calibration and interferences from $RO_2$ radicals, Atmos. Meas. Tech., 4, 1209–1225, doi:10.5194/amt-4-1209-2011, 2011. 22389

Fuchs, H., Hofzumahaus, A., Rohrer, F., Bohn, B., Brauers, T., Dorn, H.-P., Haeseler, R., Holland, F., Kaminski, M., Li, X., Lu, K., Nehr, S., Tillmann, R., Wegener, R., and Wahner, A.: Experimental evidence for efficient hydroxyl radical regeneration in isoprene oxidation, Nat. Geosci., 6, 1023–1026, doi:10.1038/ngeo1964, 2013. 22389

Ganzeveld, L., Bouwman, L., Stehfest, E., van Vuuren, D. P., Eickhout, B., and Lelieveld, J.: Impact of future land use and land cover changes on atmospheric chemistry–climate interactions, J. Geophys. Res., 115, D23301, doi:10.1029/2010JD014041, 2010. 22388

Guenther, A., Karl, T., Harley, P., Wiedinmyer, C., Palmer, P. I., and Geron, C.: Estimates of global terrestrial isoprene emissions using MEGAN (Model of Emissions of Gases and Aerosols from Nature), Atmos. Chem. Phys., 6, 3181–3210, doi:10.5194/acp-6-3181-2006, 2006. 22387, 22394

Haagen-Smit, A. J.: Chemistry and physiology of Los Angeles smog, Ind. Eng. Chem. Res., 44, 1342–1346, doi:10.1021/ie50510a045, 1952. 22387

Horowitz, L. W., Fiore, A. M., Milly, G. P., Cohen, R. C., Perring, A., Wooldridge, P. J., Hess, P. G., Emmons, L. K., and Lamarque, J.-F.: Observational constraints on the chemistry of isoprene nitrates over the eastern United States, J. Geophys. Res., 112, D12S08, doi:10.1029/2006JD007747, 2007. 22389

Huntingford, C., Cox, P. M., Mercado, L. M., Sitch, S., Bellouin, N., Boucher, O., and Gedney, N.: Highly contrasting effects of different climate forcing agents on terrestrial ecosystem services, Philos. T. Roy. Soc. A, 369, 2026–2037, doi:10.1098/rsta.2010.0314, 2011. 22388

Jeffries, H. E., Gery, M. W., and Carter, W. P. L.: Protocols for Evaluating Oxidant Mechanisms Used in Urban and Regional Models, Tech. rep., US Environmental Protection Agency, At-

mospheric Research and Exposure Assessment Laboratory, Research Triangle Park, NC 27711, 1992. 22388

Jenkin, M.: Review of the atmospheric chemistry of isoprene and evaluation of mechanisms for global modelling, Tech. rep., UK Met Office, Atmospheric Chemistry Services, Oakhampton, Devon, UK, 2012. 22391, 22392, 22398

Jenkin, M. E., Saunders, S. M., and Pilling, M. J.: The tropospheric degradation of volatile organic compounds: a protocol for mechanism development, Atmos. Environ., 31, 81–104, doi:10.1016/S1352-2310(96)00105-7, 1997. 22391, 22393

Kleinman, L., Daum, P., Lee, J., Lee, Y., Nunnermacker, L., Springston, S., Newman, L., Weinstein-Lloyd, J., and Sillman, S.: Dependence of ozone production on NO and hydrocarbons in the troposphere, Geophys. Res. Lett., 24, 2299–2302, doi:10.1029/97GL02279, 1997. 22403

Kubistin, D., Harder, H., Martinez, M., Rudolf, M., Sander, R., Bozem, H., Eerdekens, G., Fischer, H., Gurk, C., Klüpfel, T., Königstedt, R., Parchatka, U., Schiller, C. L., Stickler, A., Taraborrelli, D., Williams, J., and Lelieveld, J.: Hydroxyl radicals in the tropical troposphere over the Suriname rainforest: comparison of measurements with the box model MECCA, Atmos. Chem. Phys., 10, 9705–9728, doi:10.5194/acp-10-9705-2010, 2010. 22388

Kwok, E. S. C. and Atkinson, R.: Estimation of hydroxyl radical reaction-rate constants for gas-phase organic-compounds using a structure-reactivity relationship – an update, Atmos. Environ., 29, 1685–1695, doi:10.1016/1352-2310(95)00069-B, 1995. 22393

Lathiere, J., Hewitt, C. N., and Beerling, D. J.: Sensitivity of isoprene emissions from the terrestrial biosphere to 20th century changes in atmospheric $CO_2$ concentration, climate, and land use, Glob. Change Biol., 24, GB1004, doi:10.1029/2009GB003548, 2010. 22394

Lee, L., Teng, A. P., Wennberg, P. O., Crounse, J. D., and Cohen, R. C.: On rates and mechanisms of OH and $O_3$ reactions with isoprene-derived hydroxy nitrates, J. Phys. Chem. A, 118, 1622–1637, doi:10.1021/jp4107603, 2014. 22390

Lockwood, A. L., Shepson, P. B., Fiddler, M. N., and Alaghmand, M.: Isoprene nitrates: preparation, separation, identification, yields, and atmospheric chemistry, Atmos. Chem. Phys., 10, 6169–6178, doi:10.5194/acp-10-6169-2010, 2010. 22390, 22391

Mao, J., Ren, X., Zhang, L., Van Duin, D. M., Cohen, R. C., Park, J.-H., Goldstein, A. H., Paulot, F., Beaver, M. R., Crounse, J. D., Wennberg, P. O., DiGangi, J. P., Henry, S. B., Keutsch, F. N., Park, C., Schade, G. W., Wolfe, G. M., Thornton, J. A., and Brune, W. H.:





ACPD
14, 22385–22435, 2014

Insights into hydroxyl measurements and atmospheric oxidation in a California forest, Atmos. Chem. Phys., 12, 8009–8020, doi:10.5194/acp-12-8009-2012, 2012. 22389

McGillen, M. R., Archibald, A. T., Carey, T., Leather, K. E., Shallcross, D. E., Wenger, J. C., and Percival, C. J.: Structure-activity relationship (SAR) for the prediction of gas-phase ozonolysis rate coefficients: an extension towards heteroatomic unsaturated species, Phys. Chem. Chem. Phys., 13, 2842–2849, doi:10.1039/c0cp01732a, 2011. 22393

Müller, J.-F., Peeters, J., and Stavrakou, T.: Fast photolysis of carbonyl nitrates from isoprene, Atmos. Chem. Phys., 14, 2497–2508, doi:10.5194/acp-14-2497-2014, 2014. 22390

O'Connor, F. M., Johnson, C. E., Morgenstern, O., Abraham, N. L., Braesicke, P., Dalvi, M., Folberth, G. A., Sanderson, M. G., Telford, P. J., Voulgarakis, A., Young, P. J., Zeng, G., Collins, W. J., and Pyle, J. A.: Evaluation of the new UKCA climate-composition model – Part 2: The Troposphere, Geosci. Model Dev., 7, 41–91, doi:10.5194/gmd-7-41-2014, 2014. 22391

Pacifico, F., Folberth, G. A., Jones, C. D., Harrison, S. P., and Collins, W. J.: Sensitivity of biogenic isoprene emissions to past, present, and future environmental conditions and implications for atmospheric chemistry, J. Geophys. Res., 117, D22302, doi:10.1029/2012JD018276, 2012. 22388

Paulot, F., Crounse, J. D., Kjaergaard, H. G., Kuerten, A., St Clair, J. M., Seinfeld, J. H., and Wennberg, P. O.: Unexpected epoxide formation in the gas-phase photooxidation of isoprene, Science, 325, 730–733, doi:10.1126/science.1172910, 2009. 22389, 22392

Paulot, F., Henze, D. K., and Wennberg, P. O.: Impact of the isoprene photochemical cascade on tropical ozone, Atmos. Chem. Phys., 12, 1307–1325, doi:10.5194/acp-12-1307-2012, 2012. 22389, 22390

Peeters, J., Nguyen, T. L., and Vereecken, L.: $HO_x$ radical regeneration in the oxidation of isoprene, Phys. Chem. Chem. Phys., 11, 5935–5939, doi:10.1039/B908511D, 2009. 22389, 22391, 22395, 22400

Perring, A. E., Bertram, T. H., Wooldridge, P. J., Fried, A., Heikes, B. G., Dibb, J., Crounse, J. D., Wennberg, P. O., Blake, N. J., Blake, D. R., Brune, W. H., Singh, H. B., and Cohen, R. C.: Airborne observations of total $RONO_2$: new constraints on the yield and lifetime of isoprene nitrates, Atmos. Chem. Phys., 9, 1451–1463, doi:10.5194/acp-9-1451-2009, 2009. 22391

Poschl, U., von Kuhlmann, R., Poisson, N., and Crutzen, P.: Development and intercomparison of condensed isoprene oxidation mechanisms for global atmospheric modeling, J. Atmos. Chem., 37, 29–52, doi:10.1023/A:1006391009798, 2000. 22391





ACPD
14, 22385–22435, 2014

Ren, X., Olson, J. R., Crawford, J. H., Brune, W. H., Mao, J., Long, R. B., Chen, Z., Chen, G., Avery, M. A., Sachse, G. W., Barrick, J. D., Diskin, G. S., Huey, L. G., Fried, A., Cohen, R. C., Heikes, B., Wennberg, P. O., Singh, H. B., Blake, D. R., and Shetter, R. E.: $HO_x$ chemistry during INTEX-A 2004: Observation, model calculation, and comparison with previous studies, J. Geophys. Res., 113, D05310, doi:10.1029/2007JD009166, 2008. 22388

Sanderson, M., Jones, C., Collins, W., Johnson, C., and Derwent, R.: Effect of climate change on isoprene emissions and surface ozone levels, Geophys. Res. Lett., 30, 1936, doi:10.1029/2003GL017642, 2003. 22388

Sandu, A. and Sander, R.: Technical note: Simulating chemical systems in Fortran90 and Matlab with the Kinetic PreProcessor KPP-2.1, Atmos. Chem. Phys., 6, 187–195, doi:10.5194/acp-6-187-2006, 2006. 22393

Savage, N. H., Agnew, P., Davis, L. S., Ordóñez, C., Thorpe, R., Johnson, C. E., O'Connor, F. M., and Dalvi, M.: Air quality modelling using the Met Office Unified Model (AQUM OS24-26): model description and initial evaluation, Geosci. Model Dev., 6, 353–372, doi:10.5194/gmd-6-353-2013, 2013. 22392, 22415

Shepson, P. B., Mackay, E., and Muthuramu, K.: Henry's law constants and removal processes for several atmospheric $\beta$-hydroxy alkyl nitrates, Environ. Sci. Technol., 30, 3618–3623, doi:10.1021/es960538y, 1996. 22390

Sillman, S. and He, D. Y.: Some theoretical results concerning $O_3$-$NO_x$-VOC chemistry and $NO_x$-VOC indicators, J. Geophys. Res., 107, 4659, doi:10.1029/2001JD001123, 2002. 22394

Squire, O. J., Archibald, A. T., Abraham, N. L., Beerling, D. J., Hewitt, C. N., Lathière, J., Pike, R. C., Telford, P. J., and Pyle, J. A.: Influence of future climate and cropland expansion on isoprene emissions and tropospheric ozone, Atmos. Chem. Phys., 14, 1011–1024, doi:10.5194/acp-14-1011-2014, 2014. 22388, 22391, 22394, 22400, 22408

Stevenson, D. S., Dentener, F. J., Schultz, M. G., Ellingsen, K., van Noije, T. P. C., Wild, O., Zeng, G., Amann, M., Atherton, C. S., Bell, N., Bergmann, D. J., Bey, I., Butler, T., Cofala, J., Collins, W. J., Derwent, R. G., Doherty, R. M., Drevet, J., Eskes, H. J., Fiore, A. M., Gauss, M., Hauglustaine, D. A., Horowitz, L. W., Isaksen, I. S. A., Krol, M. C., Lamarque, J.-F., Lawrence, M. G., Montanaro, V., Müller, J.-F., Pitari, G., Prather, M. J., Pyle, J. A., Rast, S., Rodriguez, J. M., Sanderson, M. G., Savage, N. H., Shindell, D. T., Strahan, S. E., Sudo, K., and Szopa, S.: Multimodel ensemble simulations of present-day and near-future tropospheric ozone, J. Geophys. Res., 111, D08301, doi:10.1029/2005JD006338, 2006. 22396

Stone, D., Evans, M. J., Edwards, P. M., Commane, R., Ingham, T., Rickard, A. R., Brookes, D. M., Hopkins, J., Leigh, R. J., Lewis, A. C., Monks, P. S., Oram, D., Reeves, C. E., Stewart, D., and Heard, D. E.: Isoprene oxidation mechanisms: measurements and modelling of OH and $HO_2$ over a South-East Asian tropical rainforest during the OP3 field campaign, Atmos. Chem. Phys., 11, 6749–6771, doi:10.5194/acp-11-6749-2011, 2011. 22389

von Kuhlmann, R., Lawrence, M. G., Pöschl, U., and Crutzen, P. J.: Sensitivities in global scale modeling of isoprene, Atmos. Chem. Phys., 4, 1–17, doi:10.5194/acp-4-1-2004, 2004. 22388, 22389

Wang, K. and Shallcross, D.: Modelling terrestrial biogenic isoprene fluxes and their potential impact on global chemical species using a coupled LSM-CTM model, Atmos. Environ., 34, 2909–2925, doi:10.1016/S1352-2310(99)00525-7, 2000. 22387

Warwick, N. J., Archibald, A. T., Ashworth, K., Dorsey, J., Edwards, P. M., Heard, D. E., Langford, B., Lee, J., Misztal, P. K., Whalley, L. K., and Pyle, J. A.: A global model study of the impact of land-use change in Borneo on atmospheric composition, Atmos. Chem. Phys., 13, 9183–9194, doi:10.5194/acp-13-9183-2013, 2013. 22389, 22400

Whalley, L. K., Edwards, P. M., Furneaux, K. L., Goddard, A., Ingham, T., Evans, M. J., Stone, D., Hopkins, J. R., Jones, C. E., Karunaharan, A., Lee, J. D., Lewis, A. C., Monks, P. S., Moller, S. J., and Heard, D. E.: Quantifying the magnitude of a missing hydroxyl radical source in a tropical rainforest, Atmos. Chem. Phys., 11, 7223–7233, doi:10.5194/acp-11-7223-2011, 2011. 22389

Wiedinmyer, C., Tie, X., Guenther, A., Neilson, R., and Granier, C.: Future changes in biogenic isoprene emissions: how might they affect regional and global atmospheric chemistry?, Earth Interact., 10, 3, doi:10.1175/EI174.1, 2006. 22388, 22403

Wu, S., Mickley, L. J., Jacob, D. J., Logan, J. A., Yantosca, R. M., and Rind, D.: Why are there large differences between models in global budgets of tropospheric ozone?, J. Geophys. Res., 112, D05302, doi:10.1029/2006JD007801, 2007. 22389

Wu, S., Mickley, L. J., Kaplan, J. O., and Jacob, D. J.: Impacts of changes in land use and land cover on atmospheric chemistry and air quality over the 21st century, Atmos. Chem. Phys., 12, 1597–1609, doi:10.5194/acp-12-1597-2012, 2012. 22388

Xie, Y., Paulot, F., Carter, W. P. L., Nolte, C. G., Luecken, D. J., Hutzell, W. T., Wennberg, P. O., Cohen, R. C., and Pinder, R. W.: Understanding the impact of recent advances in isoprene photooxidation on simulations of regional air quality, Atmos. Chem. Phys., 13, 8439–8455, doi:10.5194/acp-13-8439-2013, 2013. 22389, 22390





ACPD
14, 22385–22435, 2014

**Table 1.** List of chemical species included in each of the isoprene mechanisms. Note that names of some of the species in AQUM were changed from the names given in Savage et al. (2013) to be consistent with the other schemes. These are as follows: "HOIPO2" = $ISO_2$, "MVK" = MACR, "MVKOOH" = MACROOH, "HOMVKO2" = $MACRO_2$.

| Species | Description | CheT | CheT2 | AQUM | LLSF |
|---|---|---|---|---|---|
| $C_5H_8$ | isoprene | X | X | X | X |
| $ISO_2$ | hydroxyperoxy radicals from $C_5H_8 + OH$ | X | X | X | |
| ISOOH | $\beta$-hydroxyhydro-peroxides from $ISO_2 + HO_2$ | X | X | X | |
| ISON | $\beta$-hydroxy alkylnitrates from $ISO_2 + NO$ and alkyl nitrates from $C_5H_8 + NO_3$ | X | X | X | |
| MACR | methacrolein, methyl vinyl ketone and other $C_4$-carbonyls | X | X | X | |
| $MACRO_2$ | peroxy radicals from MACR + OH | X | X | X | |
| MACROOH | hydroperoxides from $MACRO_2 + HO_2$ | X | X | X | |
| MPAN | peroxymethacrylic nitric anhydride and other higher peroxy-acylnitrates | X | X | | |
| HACET | hydroxyacetone and other $C_3$-ketones | X | X | | |
| NALD | nitrooxy-acetaldehyde | X | X | | |
| IEPOX | epoxydiols | | X | | |
| HPALD | hydroperoxy-aldehydes | | X | | |
| PACALD | peroxy-acid-aldehydes | | X | | |





ACPD
14, 22385–22435, 2014



CC BY

**Table 2.** Isoprene mechanism for CheT and differences between the CheT mechanism and the CheT2, AQUM and LLSF mechanisms. If a reaction is blank then it is exactly the same as in CheT, such that only the differences are shown. All rate constants ($k$) are in units of $10^{-14}$ cm$^3$ molecule$^{-1}$ s$^{-1}$. Those species not defined in Table 1 or in the main text are defined here: HCOOH = formic acid, $H_2O_2$ = hydrogen peroxide, HCHO = formaldehyde, PACALD = acylhydroperoxyaldehydes.

| Reactants | Products | | | |
|---|---|---|---|---|
| | CheT | CheT2 | AQUM | LLSF |
| $C_5H_8 + OH$ | $ISO_2$ | | | 2 $MeO_2$–1.5OH |
| $k$ | 9990 | | 10100 | |
| $C_5H_8 + O_3$ (1) | 1.95 MACR + 1.74 HCHO + 0.3 $MACRO_2$ + 0.3 $MeCO_3$ | | 2 MACR + 1.56 CO 0.44 HCHO + 0.54 $HO_2$ | 0.87 HCHO + 1.86 $MeO_2$ + 0.06 $HO_2$ + 0.05 CO |
| $k$ | 0.0004 | | 0.0006 | 0.0013 |
| $C_5H_8 + O_3$ (2) | 0.24 $MeO_2$ + 0.84 HCOOH + 0.42 CO + 0.27 $H_2O_2$ | | not included | not included |
| $k$ | 0.0004 | | | |
| $C_5H_8 + O_3$ (3) | 0.75 $HO_2$ + 0.75 OH | | 0.54 OH | not included |
| $k$ | 0.0004 | | 0.0006 | |
| $C_5H_8 + NO_3$ | ISON | ISON + $HO_2$ | ISON + $HO_2$ | not included |
| $k$ | 69.6 | | 67.8 | |
| $ISO_2$ + NO (1) | $NO_2$ + MACR HCHO + $HO_2$ | | MACR + $NO_2$ HCHO + $HO_2$ | not included |
| $k$ | 813 | | 381 | |
| $ISO_2$ + NO (2) | ISON | | not included | not included |
| $k$ | 37.5 | 32.6 | | |
| $ISO_2 + HO_2$ | ISOOH | | | not included |
| $k$ | 89.4 | | 103 | |
| $ISO_2 + ISO_2$ | 2 MACR + HCHO + $HO_2$ | 2 MACR + 2 HCHO + 2 $HO_2$ | not included | not included |
| $k$ | 200 | | | |
| $ISO_2 + MeO_2$ | not included | not included | MACR + HCHO + 2 $HO_2$ | not included |
| $k$ | | | 50 | |
| $ISO_2 + N_2$ | not included | MACR + HCHO + OH | not included | not included |
| $k$ | | $3.85 \times 10^{10}$ | | |
| $ISO_2 + O_2$ | not included | HPALD + $HO_2$ | not included | not included |
| $k$ | | $2.56 \times 10^{11}$ | | |
| MACR + $h\nu$ | $MeCO_3$ + HCHO +CO + $HO_2$ | | not included | not included |





ACPD
14, 22385–22435, 2014



CC BY

**Table 2.** Continued.

| Reactants | Products | | | |
|---|---|---|---|---|
| | CheT | CheT2 | AQUM | LLSF |
| MACR + OH (1) | $MACRO_2$ | | | not included |
| *k* | 266 | | 1880 | |
| MACR + OH (2) | $MACRO_2$ | | not included | not included |
| *k* | 510 | | | |
| MACR + $O_3$ (1) | 1.8 MGLY + 0.9 HCOOH + 0.64 $HO_2$ + 0.44 CO | | 2 MGLY + 1.52 CO 0.48 HCHO + 0.72 $HO_2$ | not included |
| *k* | 0.00013 | | 0.000199 | |
| MACR + $O_3$ (2) | 0.38 OH + 0.2 $MeCO_3$ | | 0.72 OH | not included |
| *k* | 0.00013 | | 0.000199 | |
| MACR + $O_3$ (3) | 1.8 MGLY + 0.9 HCOOH + 0.64 $HO_2$ + 0.44 CO | | not included | not included |
| *k* | 0.0000305 | | | |
| MACR + $O_3$ (4) | 0.38 OH + 0.2 $MeCO_3$ | | not included | not included |
| *k* | 0.0000305 | | | |
| MACR dry dep | included | | not included | not included |
| $MACRO_2$ + $NO_2$ + M | MPAN | | not included | not included |
| | KFPAN | KFPAN*0.107 | | |
| $MACRO_2$ + NO (1) | 2 $NO_2$ + 0.5 $MeCO_3$ + 0.5 HACET + 0.5 CO | | $NO_2$ + $HO_2$ HCHO + MGLY | not included |
| *k* | 425 | 452 | 837 | |
| $MACRO_2$ + NO (2) | MGLY + 1.5 HCHO + 1.5 $HO_2$ | | not included | not included |
| *k* | 425 | 452 | | |
| $MACRO_2$ + $HO_2$ | MACROOH | | | not included |
| *k* | 1428 | | 1479 | |
| $MACRO_2$ + $MACRO_2$ (1) | 2 HACET + 2 MGLY + HCHO + CO | | not included | not included |
| *k* | 100 | | | |
| $MACRO_2$ + $MACRO_2$ (2) | 2 $HO_2$ | | not included | not included |
| *k* | 100 | | | |
| ISON + *hν* | $NO_2$ + MACR + HCHO + $HO_2$ | | not included | not included |
| *k* | 1300 | 3340 | | |
| ISON + OH (1) | HACET + NALD | 0.78 HACET + 0.78 NALD + 0.78 $HO_2$ | MACR + $NO_2$ | not included |
| *k* | 1300 | 1940 | 4160 | |
| ISON + OH (2) | not included | 0.44 $NO_2$ + 0.44 MACR + 0.44 HCHO | not included | not included |
| *k* | | 0.00313 | | |





ACPD
14, 22385–22435, 2014



CC BY

**Table 2.** Continued.

| Reactants | Products | | | |
|---|---|---|---|---|
| | CheT | CheT2 | AQUM | LLSF |
| ISON + $O_3$ (1) | not included | NALD + OH | | |
| *k* | | 0.00607 | | |
| ISON + $O_3$ (2) | not included | MACR + HCHO<br>$NO_2$ | | |
| *k* | | 0.00313 | | |
| ISON wet dep | included | | | not included |
| ISON dry dep | included | | not included | not included |
| HCOOH + OH | $HO_2$ | | not included | not included |
| *k* | 45 | | | |
| HCOOH wet dep | included | | not included | not included |
| HCOOH dry dep | included | | not included | not included |
| ISOOH + *hv* | OH + MACR<br>+ HCHO +$HO_2$ | | OH + MACR<br>+ HCHO + $HO_2$ | not included<br>not included |
| ISOOH + OH (1) | MACR + OH | | | |
| *k* | 10000 | 894 | | |
| ISOOH + OH (2) | not included | IEPOX + OH | | |
| *k* | | 8064 | | |
| ISOOH wet dep | included | | not included | not included |
| ISOOH dry dep | included | | not included | not included |
| MPAN + *hv* | | | not included | not included |
| MPAN + M | $MACRO_2$ + $NO_2$ | | not included | not included |
| MPAN + OH | HACET + $NO_2$ | | not included | not included |
| *k* | 2900 | | | |
| MPAN dry dep | included | | not included | not included |
| HACET + *hv* | $MeCO_3$ + HCHO<br>+ $HO_2$ | | not included | not included |
| HACET + OH | MGLY + $HO_2$ | | not included | not included |
| *k* | 300 | 445 | | |
| HACET wet dep | included | | not included | not included |
| HACET dry dep | included | | not included | not included |
| MACROOH + *hv* (1) | 2OH + 2$HO_2$ | | OH + MGLY<br>+ HCHO + $HO_2$ | not included |
| MACROOH + *hv* (2) | HACET + CO<br>+ MGLY + HCHO | | not included | not included |
| MACROOH + OH | $MACRO_2$ | | MGLY + HCHO<br>+ OH | not included |
| *k* | 3000 | | 5770 | |
| MACROOH wet dep | included | | | not included |
| MACROOH dry dep | included | | | not included |
| NALD + *hv* | HCHO + CO<br>$NO_2$ + $HO_2$ | | not included<br>not included | not included<br>not included |





ACPD
14, 22385–22435, 2014



CC BY

**Table 2.** Continued.

| Reactants | Products | | | |
|---|---|---|---|---|
| | CheT | CheT2 | AQUM | LLSF |
| NALD + OH | HCHO + CO + $NO_2$ | | not included | not included |
| *k* | 1500 | 155 | | |
| NALD dry dep | included | | not included | not included |
| $MACRO_2$ + $MeO_2$ | not included | | MGLY + HCHO 2 $HO_2$ | |
| *k* | | | 200 | |
| HPALD + *hv* | not included | PACALD + $HO_2$ + OH | | |
| HPALD + OH | not included | MGLY + CO + HCHO + OH | | |
| *k* | | 7610 | | |
| IEPOX + OH | not included | $MACRO_2$ | | |
| *k* | | 913 | | |
| PACALD + *hv* | not included | CO + $HO_2$ + MGLY + OH | | |





ACPD
14, 22385–22435, 2014

**Table 3.** Near surface (below 720 m) mean $O_x$ budget fluxes (mol gc$^{-1}$ s$^{-1}$) for regions with high isoprene emissions (greater than 0.1 mg C m$^{-2}$ h$^{-1}$) and low $NO_x$ emissions (less than 0.03 mg N m$^{-2}$ h$^{-1}$). Values from the BASE run are given. Also given are the differences caused by climate change (CC) and land use change (LC). See Fig. 4 for which gridcells were used to calculate the values in this table. $\Sigma RO_2 = HO_2 + MeO_2 + RO_2$.

| Flux | CheT | | | CheT2 | | | AQUM | | | LLSF | | |
|---|---|---|---|---|---|---|---|---|---|---|---|---|
| | BASE | CC | LC | BASE | CC | LC | BASE | CC | LC | BASE | CC | LC |
| $HO_2 + NO$ | 31 | +4.6 | +3.3 | 32 | +4.4 | +3.2 | 55 | +7.8 | −2.2 | 97 | −1.8 | −16 |
| $MeO_2 + NO$ | 12 | +2.1 | +1.6 | 11.5 | +2.0 | +1.8 | 21 | +3.5 | −0.2 | 100 | −3.2 | −30 |
| $RO_2 + NO$ | 31 | +3.4 | −7.0 | 29 | +2.9 | −6.7 | 51 | +4.0 | −14 | 2.0 | +0.1 | +0.7 |
| OH + RCOOH | 0.0 | 0.0 | 0.0 | 0.0 | 0.0 | 0.0 | 0.0 | 0.1 | 0.0 | 0.1 | 0.0 | 0.0 |
| $RONO_2 + OH$ | 0.3 | +0.1 | +0.1 | 0.3 | +0.1 | 0.0 | 1.4 | +0.2 | −0.3 | 0.0 | 0.0 | 0.0 |
| $RONO_2 + h\nu$ | 0.1 | 0.0 | 0.0 | 0.4 | 0.0 | −0.1 | 0.0 | 0.0 | 0.0 | 0.0 | 0.0 | 0.0 |
| $O^1D + H_2O$ | 29 | +2.6 | +1.3 | 29 | +2.4 | +1.1 | 35 | +3.4 | −0.7 | 43 | +1.9 | −4.2 |
| Minor loss rxns | 0.0 | 0.0 | 0.0 | 0.0 | 0.0 | 0.0 | 0.0 | 0.0 | 0.0 | 0.0 | 0.0 | 0.0 |
| $HO_2 + O_3$ | 8.2 | +0.8 | −0.1 | 9.0 | +0.8 | −0.2 | 13 | +1.6 | −1.3 | 19 | −0.3 | −4.5 |
| $OH + O_3$ | 1.4 | +0.2 | +0.9 | 1.5 | +0.2 | +0.9 | 2.3 | +0.5 | +0.9 | 2.8 | +0.2 | +0.9 |
| $O_3$ + alkene | 20 | −2.6 | −11 | 19 | −2.7 | −10 | 19 | −3.0 | −11 | 18 | −3.4 | −12 |
| $N_2O_5 + H_2O$ | 0.0 | 0.0 | 0.0 | 0.0 | 0.0 | 0.0 | 0.0 | 0.0 | 0.0 | 0.2 | 0.0 | 0.0 |
| $NO_3$ Loss | 2.9 | +0.5 | −0.2 | 3.0 | +0.5 | −0.3 | 4.7 | +0.5 | −1.1 | 3.8 | 0.0 | −1.1 |
| $NO_y$ Wet Dep | 0.7 | 0.0 | +0.2 | 0.7 | 0.0 | +0.2 | 0.9 | +0.1 | +0.2 | 1.4 | −0.1 | −1.1 |
| $\Sigma RO_2 + NO$ | 74 | +10 | −2.1 | 73 | +9.3 | −1.5 | 130 | +15 | −16 | 199 | −4.9 | −45 |
| Tot. Chem Prod | 74 | +10 | −2.0 | 74 | +9.4 | −1.7 | 130 | +16 | −17 | 200 | −4.9 | −45 |
| Tot. Chem Loss | 62 | +1.6 | −8.7 | 62 | +1.3 | −8.4 | 75 | +3.0 | −13 | 89 | −1.6 | −20 |
| Net Chem | 13 | +8.6 | +6.7 | 12 | +8.0 | +6.7 | 53 | +13 | −4.0 | 110 | −3.2 | −24 |
| $O_3$ Dry Dep | 330 | +14 | +2.4 | 330 | +12 | −0.2 | 390 | +18 | −23 | 490 | −6.1 | −74 |
| $NO_y$ Dry Dep | 10 | 0.0 | −0.1 | 10 | +0.1 | 0.0 | 11 | +0.1 | −0.1 | 9.9 | +0.7 | +0.2 |





ACPD
14, 22385–22435, 2014



CC BY

**Table 4.** Whole tropospheric $O_x$ budget ($Tg\,yr^{-1}$) and $O_3$ burden (Tg) in the BASE run for different mechanisms, and changes due to climate change (CC), isoprene emissions with climate change (IC), anthropogenic emissions (AC), and land use (LC).

| Experiment | Mechanism | Prod | Loss | Net Chem | Influx | Dry Dep | Burden (Tg) |
|---|---|---|---|---|---|---|---|
| BASE | CheT | 6188 | 5706 | 482 | −673 | 1155 | 379 |
| | CheT2 | 6234 | 5742 | 492 | −662 | 1154 | 380 |
| | AQUM | 6234 | 5776 | 458 | −733 | 1191 | 374 |
| | LLSF | 5979 | 5480 | 499 | −681 | 1180 | 360 |
| CC | CheT | 361 | 540 | −179 | −165 | −14 | 380 |
| | CheT2 | 349 | 530 | −181 | −165 | −16 | 380 |
| | AQUM | 350 | 515 | −165 | −149 | −17 | 374 |
| | LLSF | 329 | 500 | −171 | −150 | −21 | 360 |
| IC | CheT | 90 | 75 | 15 | 7 | 8 | 383 |
| | CheT2 | 113 | 94 | 20 | 9 | 11 | 385 |
| | AQUM | 128 | 97 | 31 | 17 | 14 | 380 |
| | LLSF | 154 | 122 | 32 | 11 | 21 | 367 |
| AC | CheT | −196 | −131 | −65 | −30 | −35 | 379 |
| | CheT2 | −160 | −112 | −47 | −12 | −36 | 380 |
| | AQUM | −188 | −109 | −80 | −44 | −36 | 376 |
| | LLSF | −160 | −109 | −51 | −23 | −28 | 364 |
| LC | CheT | −294 | −297 | 3 | 39 | −36 | 361 |
| | CheT2 | −314 | −317 | 3 | 41 | −38 | 361 |
| | AQUM | −351 | −350 | −1 | 49 | −50 | 357 |
| | LLSF | −346 | −305 | −41 | 22 | −63 | 346 |





ACPD
14, 22385–22435, 2014



CC BY

**Table 5.** Changes in the near surface (below 720 m) mean $O_x$ budget fluxes from the IC experiment (mol gc$^{-1}$ s$^{-1}$). The budget is split into three regimes; ICr1 – $NO_x$-limited regions with large increases in isoprene emissions, ICr2 – $NO_x$-limited regions with large decreases in isoprene emissions, and ICr3 – VOC-limited regions with large increases in isoprene emissions. Please see Fig. 12 for which gridcells were included in each regime, and see text for precise definitions of the regimes.

| Flux | CheT | | | CheT2 | | | AQUM | | | LLSF | | |
|---|---|---|---|---|---|---|---|---|---|---|---|---|
| | ICr1 | ICr2 | ICr3 | ICr1 | ICr2 | ICr3 | ICr1 | ICr2 | ICr3 | ICr1 | ICr2 | ICr3 |
| $HO_2 + NO$ | −6 | +14 | +14 | −6 | +14 | +15 | +2 | −17 | +27 | +33 | −60 | +29 |
| $MeO_2 + NO$ | −3 | +9 | +1 | −3 | +9 | +1 | −1 | −3 | +5 | +58 | −93 | +27 |
| $RO_2 + NO$ | +11 | −35 | +15 | +10 | −33 | +15 | +23 | −59 | +23 | −1.4 | +3.7 | −0.9 |
| $OH + RCOOH$ | 0 | 0 | −0.2 | 0 | 0 | −0.1 | 0 | 0 | −0.1 | 0 | 0 | −0.1 |
| $RONO_2 + OH$ | −0.1 | −0.4 | +0.5 | −0.1 | −0.2 | +0.2 | −0.0 | +0.0 | −0.0 | −0.0 | +0.0 | −0.0 |
| $RONO_2 + h\nu$ | +0.0 | −0.0 | +0.0 | +0.0 | −0.4 | +0.1 | −0.0 | −0.0 | +0.0 | +0.0 | −0.0 | +0.0 |
| $O^1D + H_2O$ | −3 | 0 | +0.9 | −3 | +1 | +0.9 | −1 | −4 | +1.7 | +6 | −12 | +2.0 |
| Minor loss rxns | 0 | 0 | 0 | 0 | 0 | 0 | 0 | 0 | 0 | 0 | 0 | 0 |
| $HO_2 + O_3$ | 0 | 0 | +1.3 | 0 | −1 | +2.1 | 0 | −6 | +4.0 | +7 | −10 | +2.6 |
| $OH + O_3$ | −2 | +5 | −0.8 | −2 | +5 | −0.7 | −2 | +4 | −0.1 | −2 | +3 | −0.2 |
| $O_3$ + alkene | +22 | −16 | +1.9 | +21 | −14 | +1.6 | +24 | −15 | +1.9 | +27 | −13 | +1.7 |
| $N_2O_5 + H_2O$ | 0 | 0 | −0.3 | 0 | 0 | −0.3 | 0 | 0 | −0.3 | 0 | 0 | +0.0 |
| $NO_3$ Loss | 0 | −3 | +3.2 | 0 | −3 | +2.9 | +2 | −5 | +2.9 | +2 | −4 | +1.9 |
| $NO_y$ Wet Dep | 0 | 0 | −0.5 | 0 | 0 | −0.4 | 0 | 0 | −0.3 | 0 | 0 | −0.0 |
| $\Sigma RO_2 + NO$ | +2 | −12 | +30 | +1 | −10 | +31 | +24 | −79 | +55 | +90 | −149 | +55 |
| Tot. Chem Prod | +1.9 | −12 | +31 | +0.7 | −9.8 | +32 | +24 | −79 | +56 | +90 | −149 | +54 |
| Tot. Chem Loss | +17 | −13 | +5.7 | +16 | −11 | +6.2 | +23 | −26 | +9.8 | +40 | −36 | +7.9 |
| Net Chem | −16 | −0.4 | +25 | −16 | +1.4 | +26 | +1.1 | −53 | +46 | +50 | −113 | +47 |
| $O_3$ Dry Dep | −25 | 0 | +35 | −23 | +3 | +34 | −12 | −33 | +58 | +51 | −81 | +66 |
| $NO_y$ Dry Dep | −1 | +6 | −1.4 | −1 | +6 | −0.8 | −1 | +3 | +2.4 | −1 | +2 | +0.4 |





ACPD
14, 22385–22435, 2014



CC BY

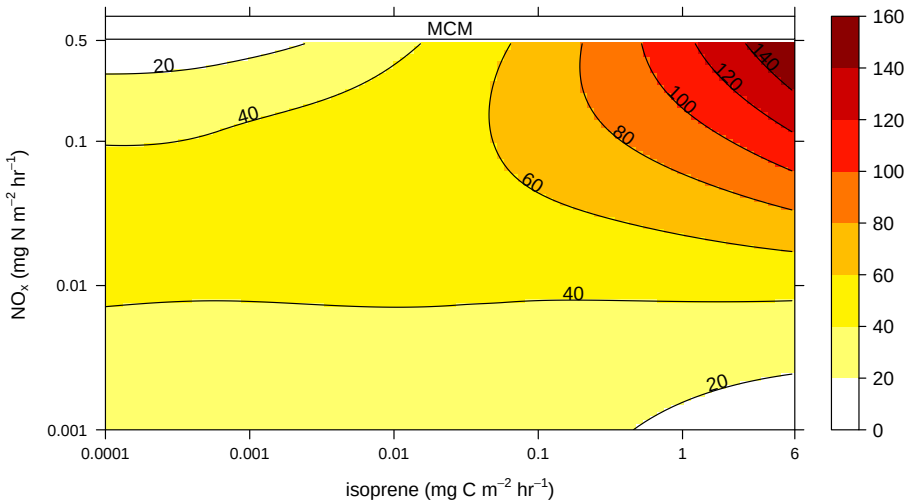


**Figure 1.** $O_3$ (ppb) isopleth plot as a function of $NO_x$ and isoprene emissions for the Master Chemical Mechanism (MCMv3.2). This was created from a series of box model runs.





ACPD
14, 22385–22435, 2014

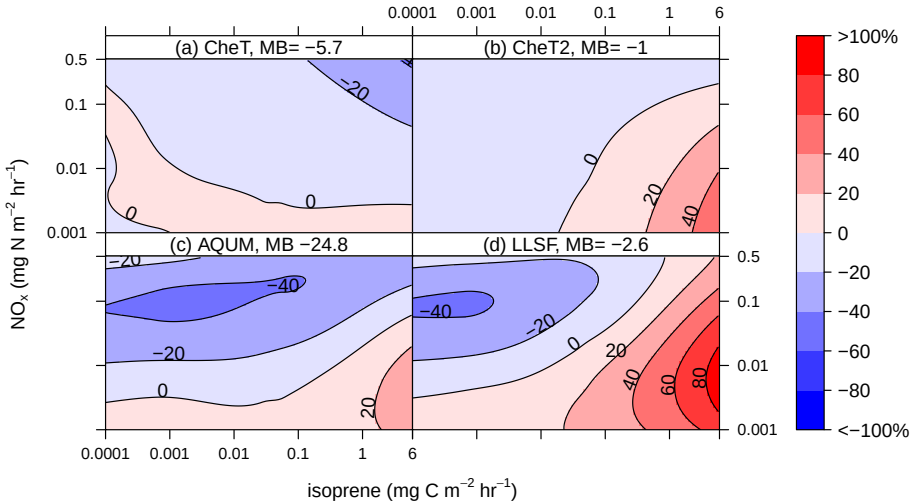


**Figure 2.** $O_3$ (percentage difference from the MCM, Fig. 1) isopleth plot as a function of $NO_x$ and isoprene emissions for different isoprene chemical mechanisms. Also quoted for each plot is the mean bias (MB) from the MCM.





ACPD
14, 22385–22435, 2014

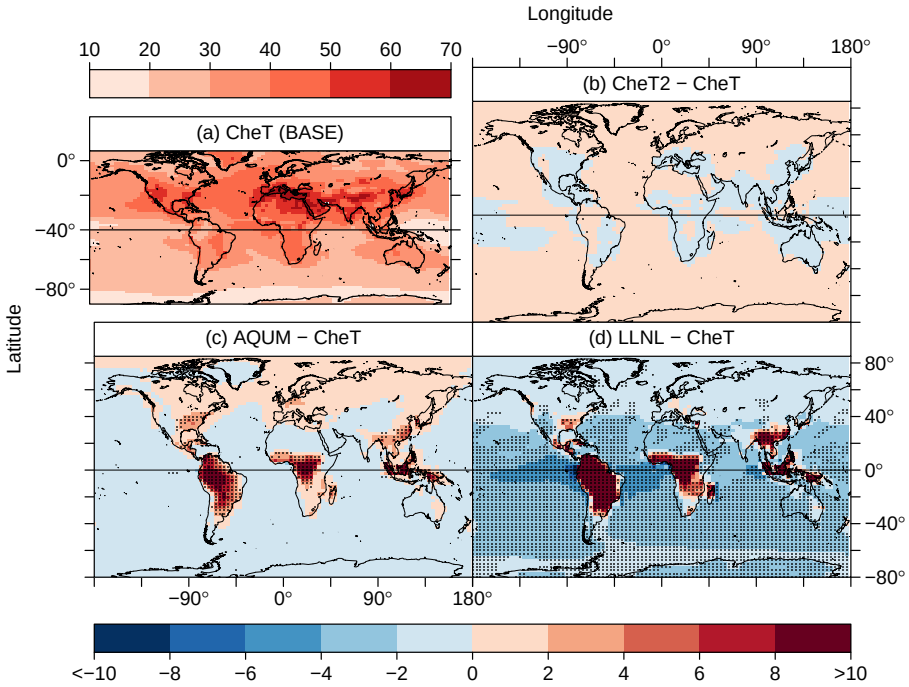


**Figure 3.** Difference in the present day (2000, BASE) five year mean near surface (< 720 m) $O_3$ (ppb) between CheT isoprene chemistry and other isoprene chemical mechanisms. Changes are considered significant (stippled) if they are greater than 2 times the standard deviation for the five year mean (i.e. approximately the 5 % level).





ACPD
14, 22385–22435, 2014

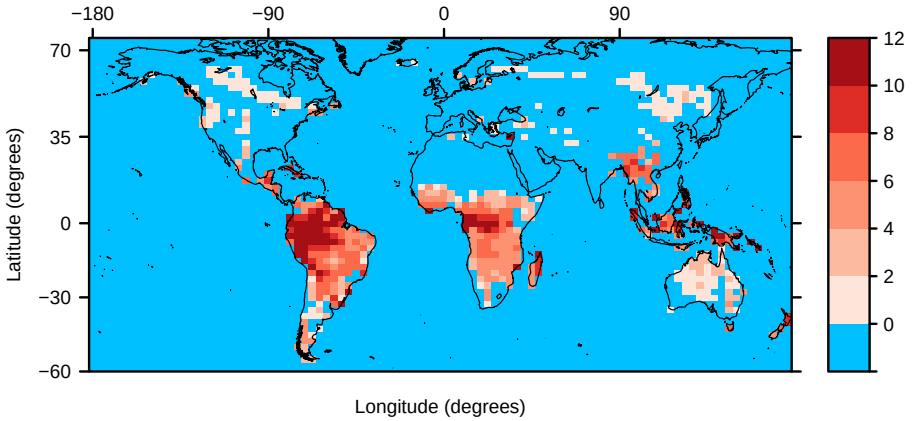


**Figure 4.** Gridcells included in the calculation of the mean $O_x$ budget fluxes reported in Table 3. Units range from 0 to 12, indicating the number of months per year that each gridcell was included in the calculation. Using emissions from the BASE run, only those months when mean isoprene emissions were greater than 0.1 mg C $m^{-2}$ $h^{-1}$ and mean $NO_x$ emissions were less than 0.03 mg N $m^{-2}$ $h^{-1}$ were included. Blue indicates that, based on this criteria, the gridcell was not included in the calculation at all.





ACPD
14, 22385–22435, 2014

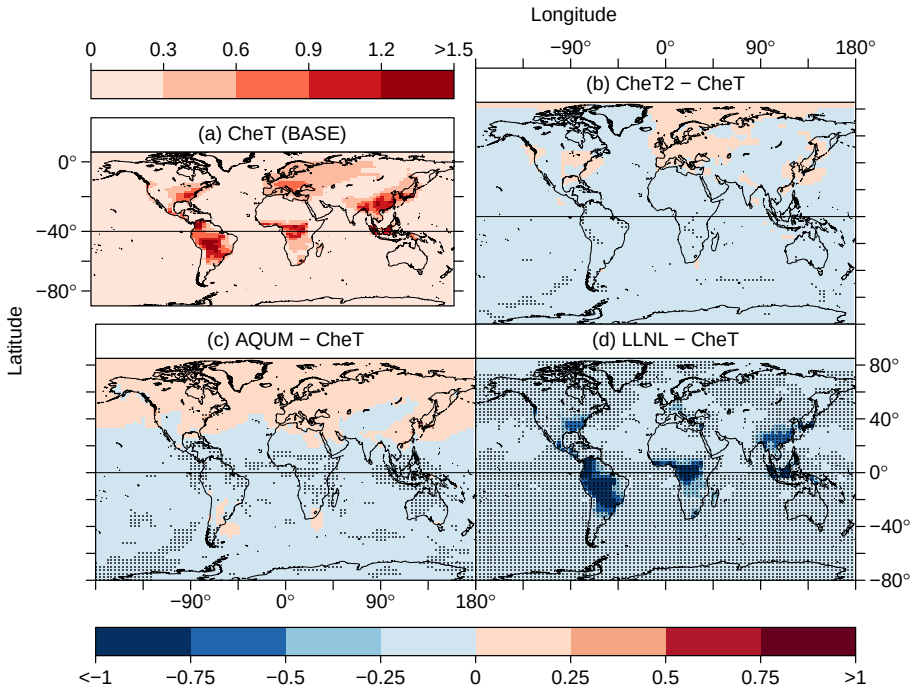


**Figure 5.** Difference in the present day (2000, BASE) five year mean near surface (< 720 m) ΣPAN (ppb) between CheT isoprene chemistry and other isoprene chemical mechanisms. Changes are considered significant (stippled) if they are greater than 2 times the standard deviation for the five year mean (i.e. approximately the 5 % level).





ACPD
14, 22385–22435, 2014

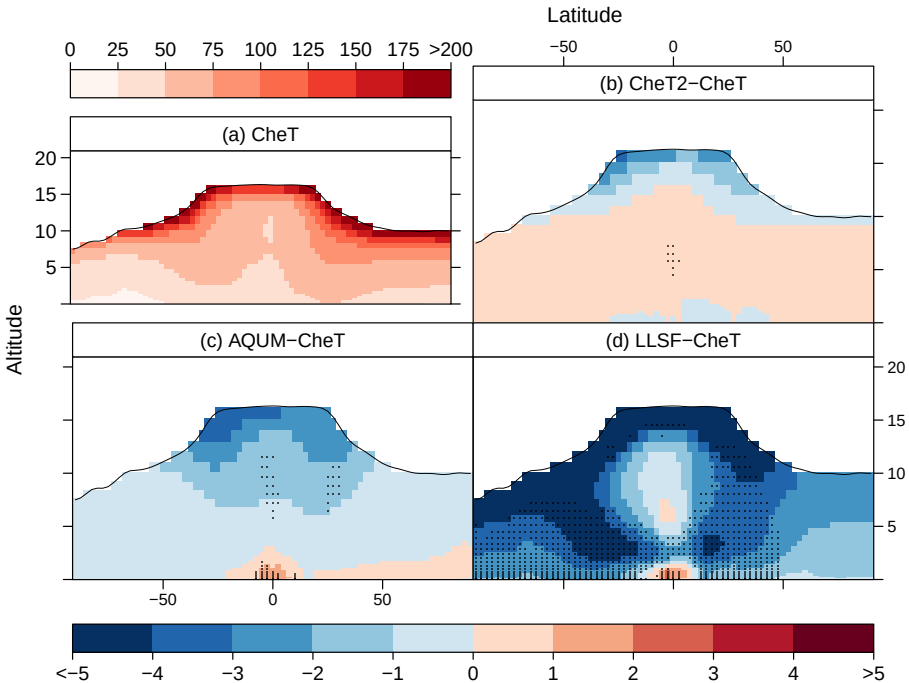


**Figure 6.** Difference in the present day (2000, BASE) five year mean zonal $O_3$ (ppb) between CheT isoprene chemistry and other isoprene chemical mechanisms. Changes are considered significant (stippled) if they are greater than 2 times the standard deviation for the five year mean (i.e. approximately the 5 % level).





ACPD
14, 22385–22435, 2014

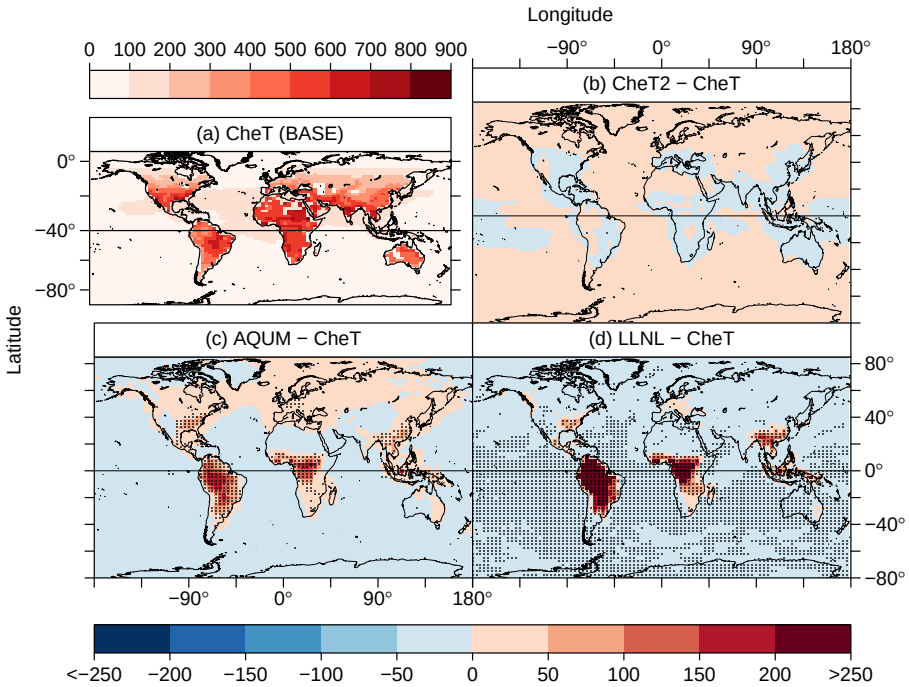


**Figure 7.** Difference in the present day (2000, BASE) five year mean $O_3$ dry deposition rate ($mol\,gc^{-1}\,s^{-1}$) between CheT isoprene chemistry and other isoprene chemical mechanisms. Changes are considered significant (stippled) if they are greater than 2 times the standard deviation for the five year mean (i.e. approximately the 5 % level).





ACPD
14, 22385–22435, 2014

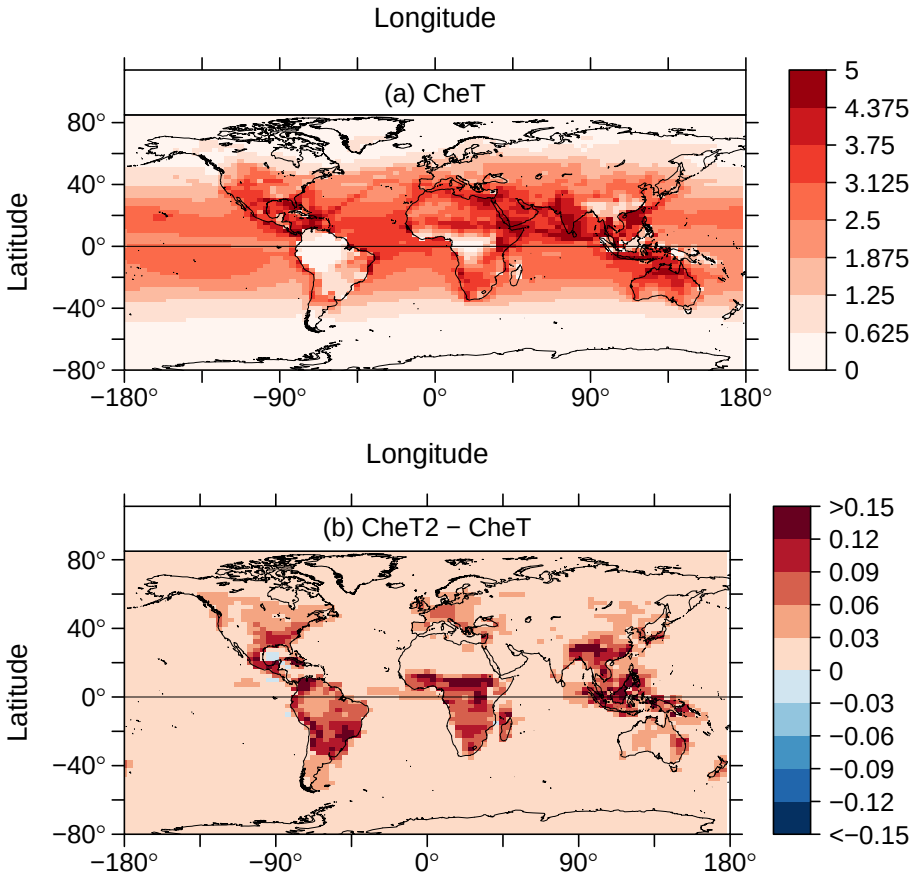


**Figure 8.** BASE five year mean near surface (below 720 m) OH ($10^6$ molecule $cm^{-3}$) in **(a)** CheT and **(b)** the difference between CheT and CheT2. Changes are considered significant (stippled) if they are greater than 2 times the standard deviation for the five year mean (i.e. approximately the 5 % level).





ACPD
14, 22385–22435, 2014



CC BY

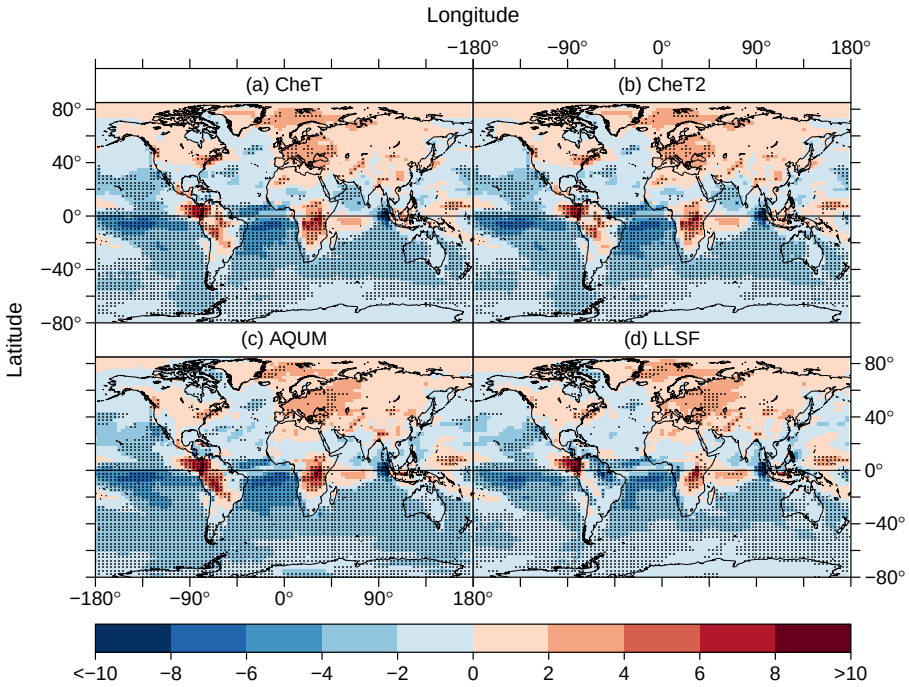


**Figure 9.** Changes in five year mean near surface (< 720 m) $O_3$ (ppb) (2095–2000) caused by climate change (CC) for different isoprene chemical mechanisms. Changes are considered significant (stippled) if they are greater than 2 times the standard deviation for the five year mean (i.e. approximately the 5 % level).





ACPD
14, 22385–22435, 2014

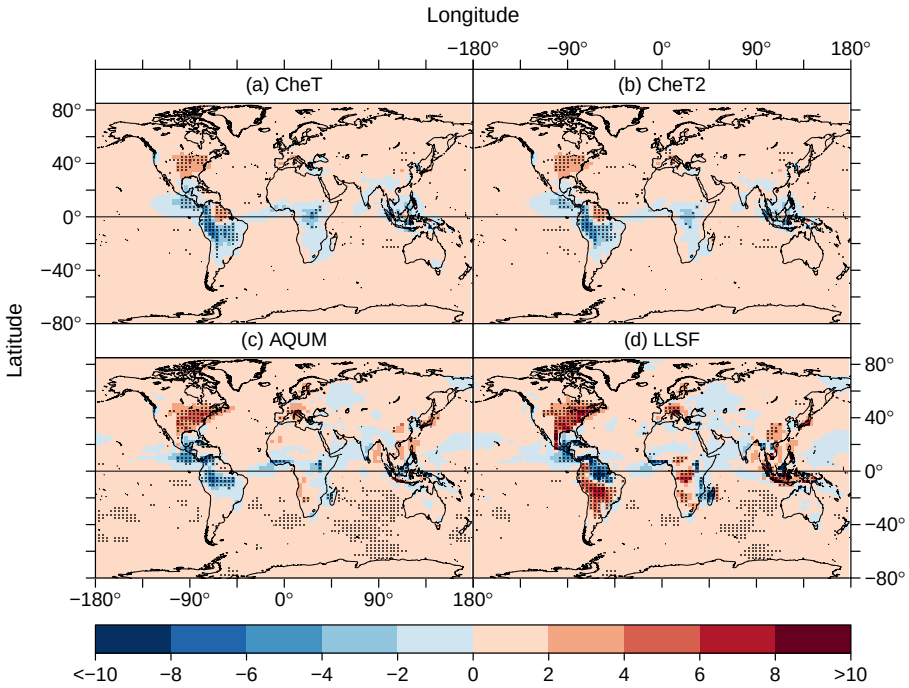


**Figure 10.** Changes in five year mean near surface (< 720 m) $O_3$ (ppb) (2095–2000) caused by the change in isoprene emissions with climate (IC) for different isoprene chemical mechanisms. Changes are considered significant (stippled) if they are greater than 2 times the standard deviation for the five year mean (i.e. approximately the 5 % level).





ACPD
14, 22385–22435, 2014

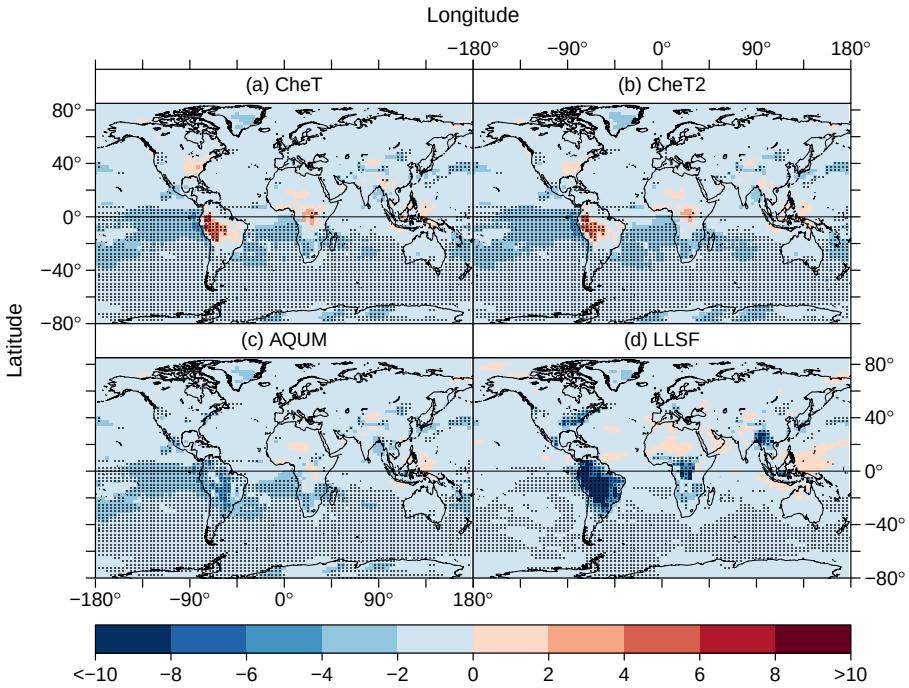


**Figure 11.** Changes in five year mean near surface (< 720 m) $O_3$ (ppb) (2095–2000) caused by land use change (LC) for different isoprene chemical mechanisms. Changes are considered significant (stippled) if they are greater than 2 times the standard deviation for the five year mean (i.e. approximately the 5 % level).





ACPD
14, 22385–22435, 2014

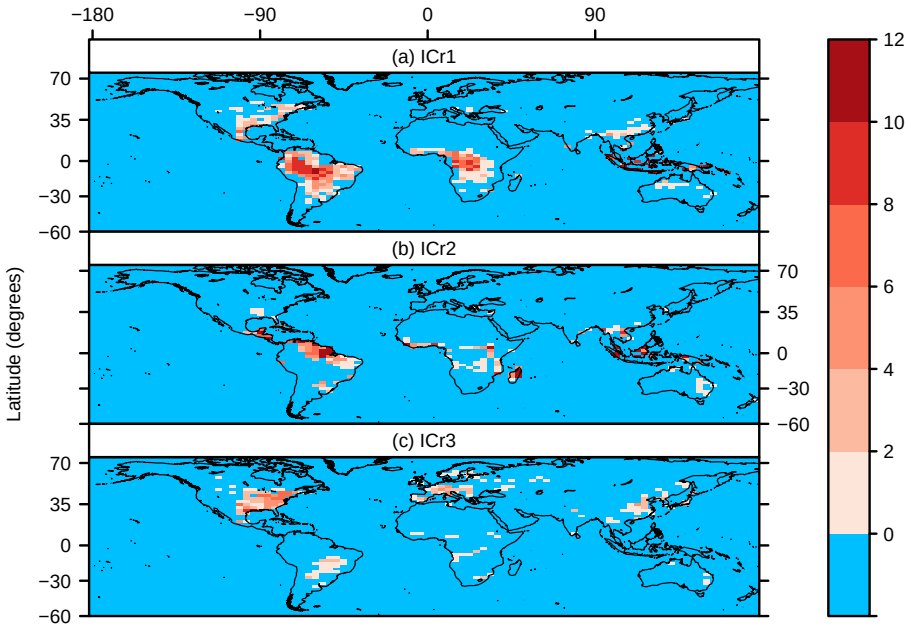


**Figure 12.** Gridcells included in the calculation of the mean $O_x$ budget fluxes reported in Table 5. Units range from 0 to 12, indicating the number of months per year that each gridcell was included in the calculation. For each region (ICr1, ICr2 and ICr3) different criteria were used to select which months a gridcell should be included, as follows: **(a)** ICr1 = months when isoprene emissions increase by more than 0.05 Tg and the environment is $NO_x$-limited. **(b)** ICr2 = months when isoprene emissions decrease by more than 0.05 Tg and the environment is $NO_x$-limited. **(c)** ICr3 = months when isoprene emissions increase by more than 0.005 Tg and the environment is VOC-limited. See text for how $NO_x$-limited and VOC-limited are defined. Blue indicates that, according to the above criteria, the gridcell was not included in the calculation at all.





ACPD
14, 22385–22435, 2014

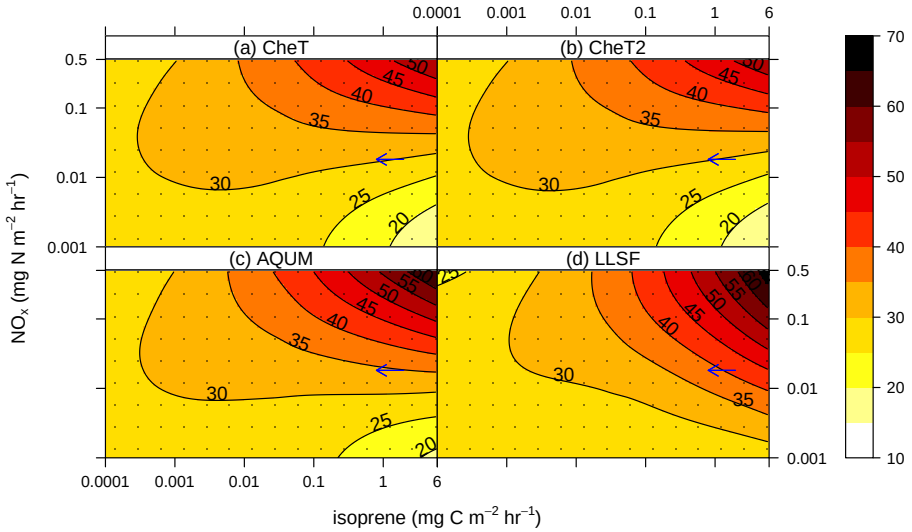


**Figure 13.** Monthly mean surface $O_3$ (ppb) as a function of monthly mean $NO_x$ and isoprene emissions from UM-UKCA. Data from all of the UM-UKCA experiments in this study is used to generate this plot. The $NO_x$ and isoprene emission rates used are identical to those used in Figs. 1 and 2.





ACPD
14, 22385–22435, 2014